

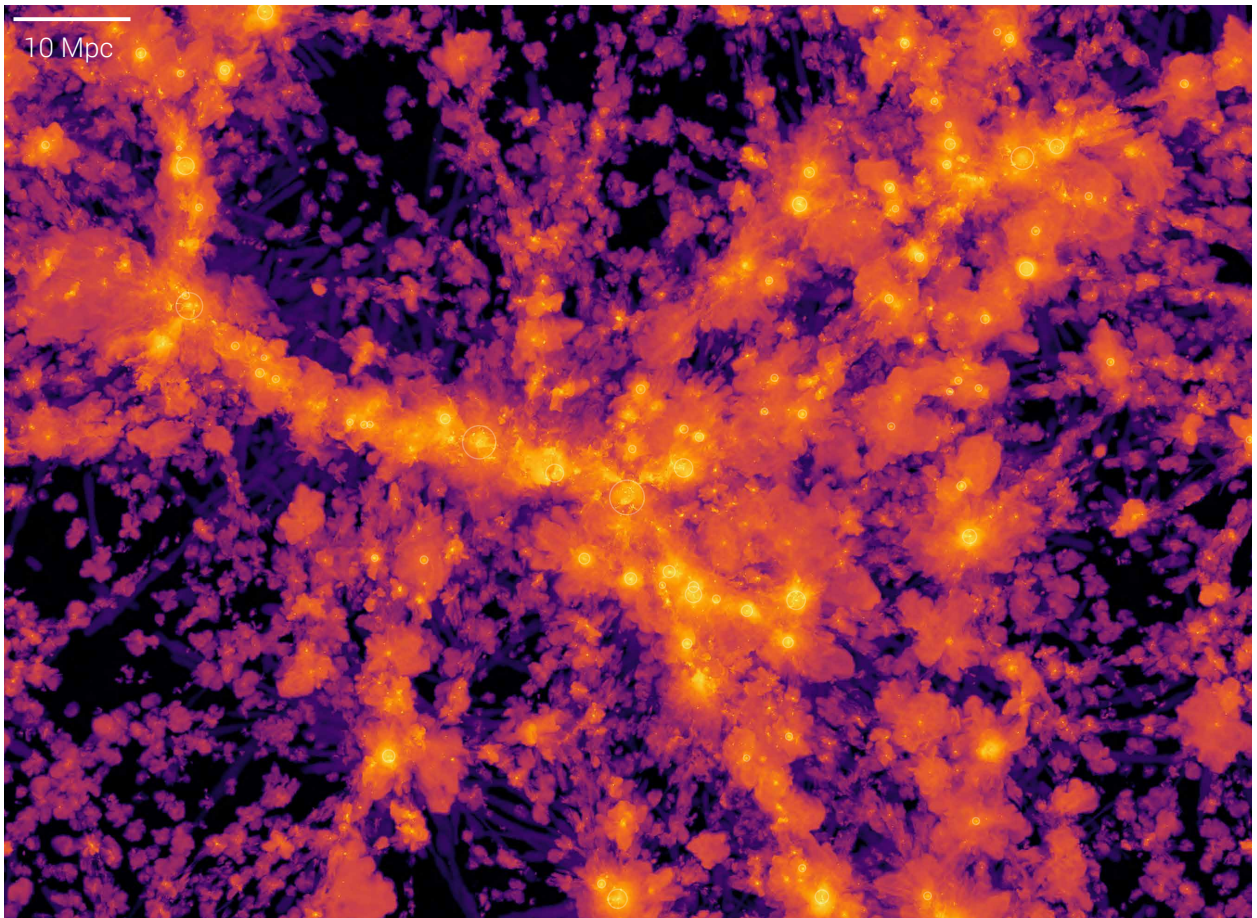
Voyage through the Hidden Physics of the Cosmic Web

Aurora Simionescu

SRON Netherlands Institute for Space Research
Sorbonnelaan 2, 3584 CA Utrecht, The Netherlands

a.simionescu@sron.nl

+31887775725



OVII X-ray surface brightness from the IllustrisTNG Simulation

Members of the Proposing Team

A. Simionescu	SRON Netherlands Institute for Space Research & Leiden Observatory, the Netherlands & Kavli IPMU, University of Tokyo, Japan
S. Ettori	INAF-OAS Bologna, Italy
N. Werner	MTA-ELTE Lendület Hot Universe research group, Hungary & Masaryk University, Czech Republic
D. Nagai	Yale University, USA
F. Vazza	University of Bologna, Italy
H. Akamatsu	SRON Netherlands Institute for Space Research
C. Pinto	ESA, the Netherlands
J. de Plaa	SRON Netherlands Institute for Space Research
N. Wijers	Leiden Observatory, the Netherlands
D. Nelson	Max Planck Institute for Astrophysics, Germany
E. Pointecouteau	IRAP, CNRS, CNES, Université de Toulouse, France
G. W. Pratt	CEA, CNRS, Université Paris-Saclay, France
D. Spiga	Stanford / SLAC, USA
E. Lau	University of Miami, USA
M. Rossetti	INAF-IASF Milano, Italy
F. Gastaldello	INAF-IASF Milano, Italy
V. Biffi	Harvard-Smithsonian Center for Astrophysics, USA
E. Bulbul	Max Planck Institute for Extraterrestrial Physics, Germany
J. W. den Herder	SRON Netherlands Institute for Space Research
D. Eckert	University of Geneva, Switzerland
F. Fraternali	Kapteyn Astronomical Institute, University of Groningen, the Netherlands
B. Mingo	The Open University, UK
G. Pareschi	INAF-OA Brera-Merate, Italy
G. Pezzulli	ETH Zürich, Switzerland
T. H. Reiprich	University of Bonn, Germany
J. Schaye	Leiden Observatory, the Netherlands
S. Walker	University of Alabama in Huntsville, USA
J. Werk	University of Washington, USA

We thank F. Nicastro, J.S. Kaastra, M. Voit, M. Donahue, J. Green, W. Cui, N. Hatch, D. Fielding, J. Sayers, J. P. Breuer, L. di Mascolo, F. Mernier and J. Croston, in no particular order, for fruitful discussions and support towards preparing this manuscript.

1 Diffuse matter in the post-*Athena* era

Most of the Universe is invisible: 95% of its contents consist of dark matter and dark energy, which we do not yet understand. But even when it comes to the “normal” standard-model particles, we can only see the tip *of the tip* of the iceberg. A large fraction of the baryons have not been converted into stars, but instead reside in the hot, diffuse medium that fills extended galaxy halos, galaxy groups, galaxy clusters, and the cosmic web. These environments are best probed by observations at soft X-ray wavelengths ($\sim 10 - 100 \text{ \AA}$), requiring spaceborne observatories.

The majority of X-ray observations so far have naturally focused on the densest, brightest centers of clusters and groups of galaxies, revealing in detail the physics of only a tiny fraction of the hot, diffuse matter that permeates the Universe. Even there, after 20 years of exquisite observations and discoveries with *Chandra* and *XMM-Newton*, many questions still loom. High-resolution X-ray spectroscopy studies of the intra-cluster medium (ICM) are all but lacking, leaving a huge gap in our knowledge of the dynamical nature of this hot, diffuse plasma. The Athena observatory is set to revolutionize this field, and significantly advance our understanding of the “Hot Universe”.

To reveal how the cosmic web is interconnected, we must **survey and physically characterize the vast majority of the very faint warm-hot diffuse baryons in the local Universe**. This poses unique challenges that no existing or planned telescope has been designed to address thus far.

What are we still missing?

1. All of the X-ray instruments approved so far only aim to measure the properties of the ICM in massive galaxy clusters within a limited radial range, typically up to r_{200c} ¹. Mapping the physics, kinematics, and chemistry within the *entire* hot gaseous halo of a single, massive, $M_{\text{virial}} \sim 10^{15} M_{\odot}$, $z=0.1$ galaxy cluster, expected to extend 4–5 times further than r_{200c} and thus cover more than 5 deg^2 on the sky, would require a whopping mosaic of 1000 pointings with the *Athena* X-IFU, most of these with an exposure time well in excess of 1 Ms (meaning a total observing time of over 30 years). **The most exciting, out-of-equilibrium parts of galaxy clusters, located beyond the virial radius and which are live witnesses to the physics of cosmic accretion, would remain entirely unexplored** in the absence of a new X-ray mission with a significantly larger grasp.
2. Massive, X-ray bright clusters of galaxies are rare, and represent only a small fraction of the matter in the Universe. The far less massive, and far fainter, **soft X-ray emitting halos of $\sim L^*$ galaxies are poorly understood, although it is in these halos that most of the stars and metals in the Universe were formed**. The dominant emission from these lower-mass halos are in the OVII and OVIII multiplets, where the resolving power of *Athena*’s X-IFU, while excellent and unprecedented at higher energies, is only $R \sim 300$. This is insufficient to measure typical velocities of $\sim 100 \text{ km/s}$ expected to be associated with the cycling of baryons through the circumgalactic medium (CGM). We need a future X-ray mission that will revolutionize the studies of the CGM in galaxies with masses similar to that of the Milky Way, in the same way that *Athena* will revolutionize studies of clusters of galaxies.
3. The diffuse matter permeating large-scale structure (LSS) filaments remains elusive. *Athena* will allow a first systematic study of this so-called Warm-Hot Intergalactic Medium (WHIM), by detecting it in absorption along 200 sightlines towards bright BLLacs and gamma-ray bursts (GRB), and studying its corresponding emission spectrum in a handful of cases. However, these observations are contingent upon the chance existence of bright (and thus rare) background beacons to illuminate the WHIM, and will only probe its properties along sparse and narrow pencil-beam sight lines. **Obtaining a complete 3D picture of the baryons permeating**

¹the radius within which the mean enclosed density is 200 times the critical density at the redshift of the cluster

the spatially complex large-scale structure requires wide-field, very sensitive tomographic observations of soft X-ray emission, in combination with absorption studies that can make use of much fainter background sources offering a more uniform sky coverage.

The CGM, cluster outskirts, and WHIM are intimately interrelated. Like blood circulating through the human body, the chemical elements produced in stars, pumped by the energy from supernovae (SNe) and supermassive black holes (SMBH), cycle through the Universe’s large-scale structure. Metals often escape the shallow gravitational potential wells of the galaxies where they were produced; from there, they either get re-accreted into the CGM, or become mixed into the diffuse LSS filaments and are then funneled into the outskirts of galaxy clusters, the most massive knots of the cosmic web. To really connect the dots of the large-scale structure and to understand this circulation in detail we need a **Cosmic Web Explorer** that will reach unprecedented X-ray sensitivity limits over unprecedented areas on the sky. Beyond a much larger mirror collecting area and field of view (FoV), a much lower and more stable instrumental background, and an improved spectral resolution at the OVII and OVIII lines, this also requires a very accurate understanding of the X-ray halo of our own Milky Way which acts as a foreground to the faint emission we are searching for. **Only a next-generation mission that will survey a large area of the sky using sensitive, high spatial and spectral resolution, integral field spectroscopy in the soft X-ray band, can fully achieve this goal, building upon previous progress brought about by XRISM² and Athena³.**

2 The unknowns of the unseen cosmic web in X-ray light

2.1 The emergent large-scale structures around the knots of the cosmic web

Galaxy clusters are the ultimate manifestation of hierarchical structure formation, and they continue to grow and accrete matter at the present time. The outer regions of galaxy clusters are home to the majority of the diffuse gas in these systems, and bear witness to the complex physics of large-scale structure growth as it happens. A plethora of unexplored structure formation physics is believed to be operating near and beyond the virial radii of galaxy clusters, and these processes are fundamentally different from the physics in the cores of clusters that has been the focus of X-ray cluster science over the past several decades.

An ultimate census of the baryons, even inside massive clusters of galaxies, can only be achieved by (1) mapping the entire volume of clusters in order to identify and characterize substructures on both small and large scales, and (2) accounting for bulk and turbulent gas motions, unresolved clumping, and non-equilibrium phenomena that would otherwise significantly bias the gas density, temperature, metal and mass measurements. **The rich thermal, kinematic and chemical contents of cluster outskirts are the Rosetta stone for understanding the growth of galaxy clusters and their connections to the Cosmic Web, as well as a stepping stone towards exploring the outskirts of massive galaxies and galaxy groups.**

2.1.1 The shocked baryons at the edge of galaxy clusters

The outermost boundary of the X-ray emitting gas halo of galaxy clusters is marked by the so-called “accretion shock” or “external shock”. It is here, around 4–5 r_{200c} , that low-temperature, low-density gas accreting from the void regions is heated by strong shocks with Mach numbers of several tens to hundreds, reaching X-ray emitting temperatures during its first infall into the cluster potential (e.g. Ryu et al., 2003; Molnar et al., 2009). “Internal shocks” or “virial shocks” due to mergers and filamentary accretion further increase the entropy of the gas. **Although directly**

²<https://global.jaxa.jp/projects/sas/xrism/>

³<https://www.the-athena-x-ray-observatory.eu/>

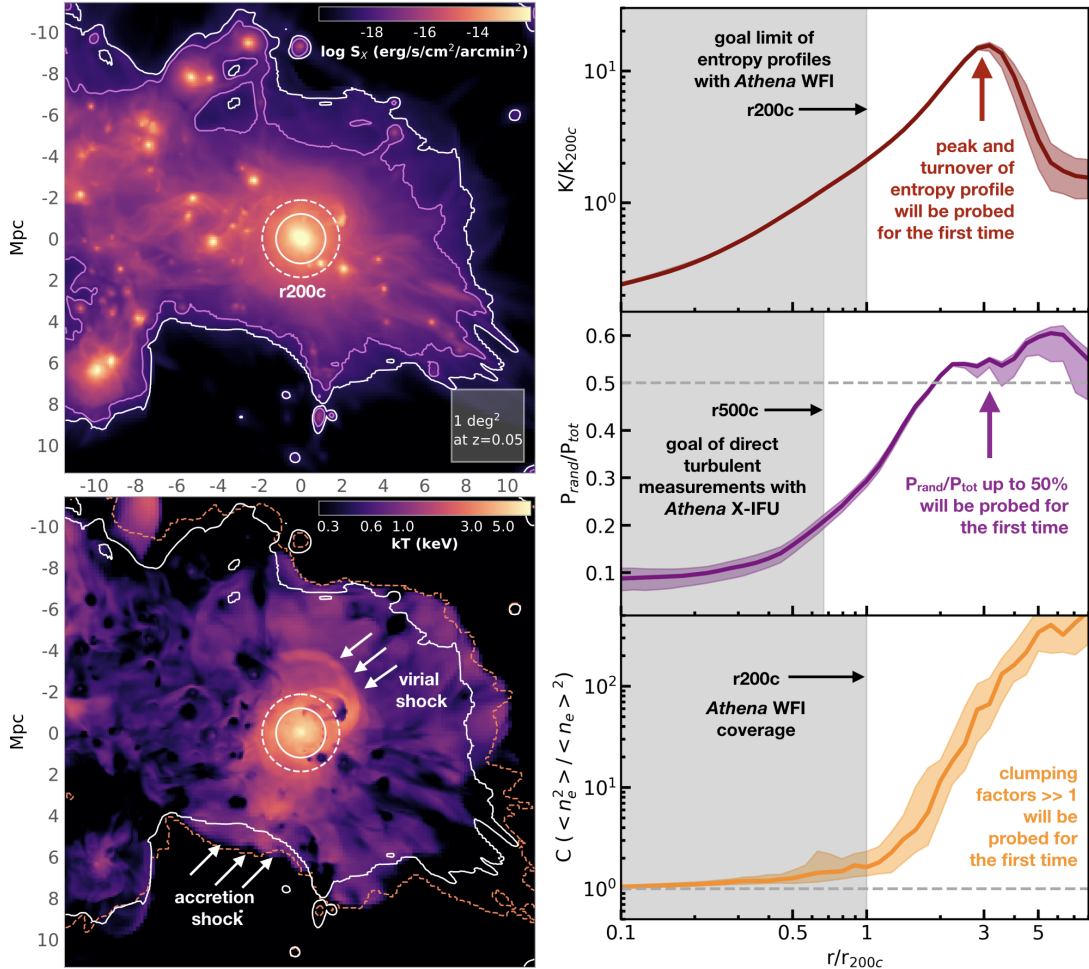


Figure 1: Example of a massive, relatively relaxed cluster from the *Omega500* adiabatic cosmological simulation (Nelson et al., 2014). Top left: predicted X-ray emissivity in the 0.5–2 keV band. Purple contours show $S_X > 10^{-18}$ erg s⁻¹ cm⁻² arcmin⁻², corresponding to the spectral simulations in Figure 2. Assuming an accurate understanding of the cosmic foregrounds and backgrounds, in an exposure time of 1 Ms the proposed mission can reach $S_X > 2 \times 10^{-19}$ erg s⁻¹ cm⁻² arcmin⁻² (white contours) over an extraction region of 1000 arcmin² at the 5σ level. Bottom left: projected temperature. Surface brightness contours at $S_X > 2 \times 10^{-19}$ erg s⁻¹ cm⁻² arcmin⁻² (white) and for a column density of $N_H > 8 \times 10^{18}$ cm⁻² (orange; to be probed in absorption against any bright quasars in the FoV) are shown. Solid and dashed circles show r_{500c} and r_{200c} , respectively. Right panel: predicted radial profiles of the entropy, ratio of the turbulent to total pressure, and gas density clumping factor in the ICM for the *Omega500* cluster sample, illustrating that the observations proposed here will probe a new regime of virialization and deviations from equilibrium that has never been reached before.

responsible for heating most of the baryons in the Universe into a hot and diffuse state, neither “virial shocks” nor “accretion shocks” have ever been probed observationally.

How did the hot universe become hot? To really understand the process of virialization and heating of the ICM, we need direct measurements probing the peak and turnover of the entropy profile at and beyond the virial radius of the cluster (as shown in the top-right panel in Figure 1). For a massive, $M_{virial} \sim 10^{15} M_\odot$ cluster, this requires reaching surface brightness levels as faint as $S_X < 10^{-18}$ erg/s/cm²/arcmin² in the 0.5–2 keV energy band, for temperatures around $kT \sim 0.6$ keV (with lower S_X and kT for lower-mass halos). Figure 2 shows the feasibility and challenges of reaching such faint flux levels.

2.1.2 Unveiling the rain and streams of plasma accreted from the surrounding LSS

Both numerical simulations and observations show that deviations from a smooth, spherical distribution become increasingly important towards the outer edges of clusters of galaxies, with inhomogeneities manifesting themselves over a broad range of spatial scales (for a recent review, see Walker et al. 2019). On large scales, high density, low entropy streams of gas from cosmic web filaments, coherent over mega-parsec scales, are predicted to penetrate deep into the cluster interior, generating bulk and turbulent gas motions, and producing shocks and contact discontinuities as they interact with the surrounding, virialized ICM (Zinger et al., 2016, 2018). On smaller scales, infalling gas substructures around tens of kpc across lead to gas clumping that is ubiquitous throughout the cluster outskirts (e.g. Nagai & Lau, 2011; Zhuravleva et al., 2013; Roncarelli et al., 2013; Vazza et al., 2013; Battaglia et al., 2015). The contributions of these infalling clumps to X-ray emission increases toward the low-density region in cluster outskirts, where they are less efficiently disrupted by ram-pressure stripping from the surrounding ICM. At present, largely due to their low surface brightness, the physical properties of these gas clumps and streams remain almost completely unexplored.

How is matter funneled into the most massive knots of the cosmic web? How and when does the accreted matter mix with the rest of the ICM? All existing major X-ray telescopes have, by now, dedicated extensive amounts of exposure time to understanding the thermodynamical properties of the ICM in the cluster outskirts, using *Suzaku* (Urban et al., 2014; Simionescu et al., 2013, 2017), *Chandra* (Morandi & Cui, 2014), and combining *XMM-Newton* and Sunyaev-Zel'dovich (SZ) measurements with *Planck* (Ghirardini et al., 2019; Ettori et al., 2019). These observations have given us a first taste of the richness of cluster outskirts physics, revealing the onset of an increasingly inhomogeneous gas density (Simionescu et al., 2011; Eckert et al., 2012, 2015a; Tchernin et al., 2016), and multiple large-scale structure filaments connecting massive clusters to the cosmic web (Werner et al., 2008; Eckert et al., 2015b; Connor et al., 2018).

But this is just the beginning. **Numerical simulations predict that the signatures of gas clumping become more and more dominant as we move beyond r_{200c} , into a radial regime that has yet to be probed by X-ray observations (as shown in the bottom-right panel of Figure 1).** The Cosmic Web Explorer will map the X-ray emissivity in galaxy clusters 3 – 5 times further in radius than the *Athena* Wide Field Imager (WFI), out to the edge of their X-ray halos marked by the accretion shock. With its large grasp (16 times that of the WFI), a lower and more stable instrumental background, and maintaining a sufficient spatial resolution (5") to identify both small-scale and large-scale asymmetries, **the proposed mission will reveal the full picture of large-scale structure formation that is currently hidden from us.**

2.1.3 Turbulence and non-thermal pressure in the regions of ongoing virialization

The continuous accretion of gas and dark matter from the Cosmic Web is expected to convert a non-negligible fraction of the infall kinetic energy into the injection of *non-thermal* energy across a wide range of scales. Recent simulations and observations indicate that the bulk of the non-thermal energy resides in subsonic chaotic gas motions in the ICM. These gas motions provide non-thermal pressure support against gravity, supplemental to thermal pressure. They are also a source of heat: kinetic energy is transported to smaller scales via progressively smaller vortices, and converted into thermal energy at the dissipation scale (< 1 kpc) (e.g., Gaspari et al., 2014; ZuHone et al., 2016; Shi et al., 2018).

To date, X-ray and SZ observations have provided early, indirect evidence for the non-thermal pressure due to bulk and turbulent gas motions in nearby clusters, from their cores (Zhuravleva et al., 2014) out to intermediate and large radii (Khatri & Gaspari, 2016; Eckert et al., 2017; Siegel et al., 2018; Eckert et al., 2019). The best direct measurements of bulk and turbulent gas velocities in the ICM to date have been obtained for the core of the Perseus cluster, where the *Hitomi* X-ray

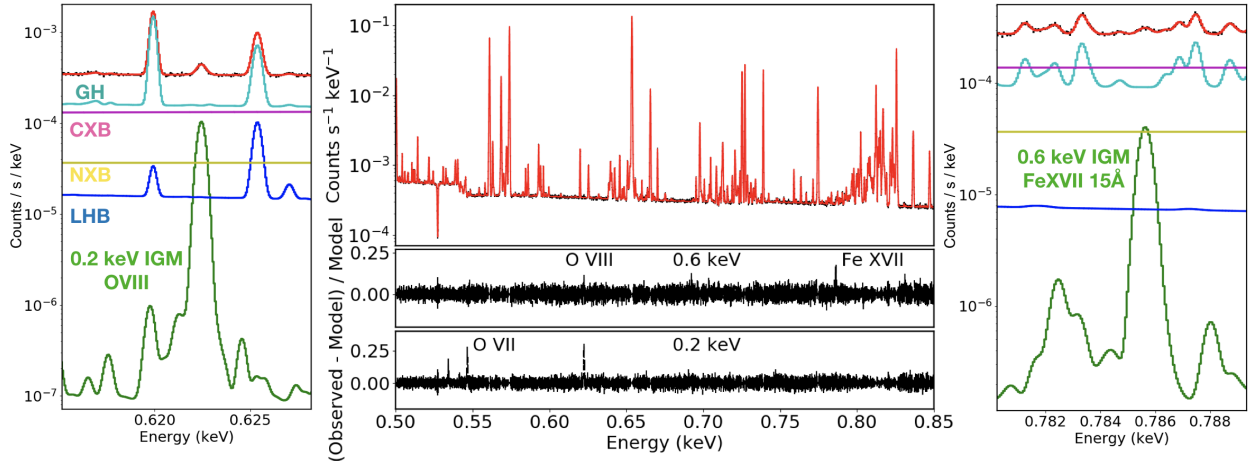


Figure 2: Simulations of faint, diffuse emission with a source surface brightness of 10^{-18} erg/s/cm²/arcmin² in the 0.5–2 keV band, metallicity of 0.3 Solar, and turbulent broadening of 100 km/s. We include the Galactic halo (GH), local hot bubble (LHB), and cosmic and instrumental X-ray backgrounds (CXB and NXB), and assume an exposure time of 1 Ms with the proposed mission configuration, and an extraction area of 1000 arcmin². Residual plots in the bottom middle panels show that several emission lines will be significantly detected for a range of temperatures typical inside the cluster accretion shock (0.6 keV, Fig. 1) and denser parts of the WHIM (0.2 keV). By covering a large sky area with high sensitivity, the proposed mission will uniquely allow us to map and model the emission from the Galaxy and unresolved AGN at the sub-percent level accuracy required for a robust characterization of the source signal.

observatory provided constraints on the Doppler shifting and broadening of the 6.7 keV Fe XXV $K\alpha$ emission line with a spectral resolution of ~ 5 eV (Hitomi Collaboration et al., 2018b). This led to important physical insights into the nature of gas motions driven by mergers and accretion, and feedback from the active galactic nucleus (AGN) (Lau et al., 2017; Bourne & Sijacki, 2017). In the coming years, *XRISM/Resolve* and the *Athena/X-IFU* will extend measurements of the bulk and turbulent motions in the ICM to many other nearby galaxy clusters, to intermediate cluster radii ($< 0.6r_{200c}$), and to the cores ($< 0.1r_{200c}$) of higher redshift clusters. This will allow us to characterize the hydrostatic mass bias due to non-thermal pressure (Ota et al., 2018), and calibrate galaxy clusters as exquisite probes for precision cosmology; the ICM velocity power spectrum will be measured with *Athena* down to several kpc scales, revealing the kinematics of the ICM close to the dissipation scale in nearby clusters (Roncarelli et al., 2018; Cucchetti et al., 2019).

Numerical simulations show that the fraction of non-thermal pressure due to gas motions increases with distance from the cluster centers (e.g., Lau et al., 2009; Vazza et al., 2018), and can become comparable to the thermal gas pressure at distances ($> r_{200c}$) that remain out of reach for all currently planned and proposed X-ray observatories (as shown in the middle right panel of Figure 1). The non-thermal pressure fraction is also a sensitive indicator of the mass accretion rate of dark matter halos (e.g., Nelson et al., 2014; Shi et al., 2015).

By combining exquisite sensitivity to faint, diffuse emission, a large FoV, and sufficient spectral resolution to detect a turbulent broadening of ~ 100 km/s for the low-energy emission lines characteristic of cluster outskirts (e.g. FeXVII, see Fig. 2), the proposed X-ray mission is equipped with the ideal capabilities to answer questions like: **How does the ongoing accretion shape the kinematic properties of the ICM near and beyond the cluster virial radii? How can we characterize the physics of the gas far out of hydrostatic equilibrium, with comparable thermal and turbulent pressures? To what extent is the dissipation of turbulence a potential heating source that supplements the virial shocks?**

2.1.4 The chemical enrichment recipe for the diffuse intergalactic baryons

Supernovae and supermassive black holes drive galactic winds, spreading the metals produced in stars into the surrounding intergalactic medium. By measuring how far these metals are spread, how many metals escape the halo of their host galaxy and when this process occurs, and by determining the relative chemical composition between various light and heavy elements, we obtain powerful probes of the properties of stellar- and AGN-driven winds, the integrated star formation history, and the physics of supernova explosions.

The ICM offers an exceptionally clean probe to measure the chemical evolution of the Universe as a whole (for a recent review, see Mernier et al. 2018a). Since the ICM plasma is well approximated as optically thin and in collisional ionization equilibrium, the equivalent widths of detected emission lines can be easily converted into elemental abundances. A relatively narrow energy band spanning 0.3–3 keV is expected to contain a wealth of line emission from elements between C and Ni.

In particular, the metallicity distribution in the outskirts of galaxy clusters is emerging as an important test bed of feedback physics, wherein the uniform level of chemical enrichment observed throughout the outer regions of massive clusters (Werner et al., 2013; Urban et al., 2017) requires a significant injection of metals from SMBH at early times (Biffi et al., 2018). The relative composition of various elements of the ICM also places constraints on the star formation histories and the chemical evolution of the universe (Simionescu et al., 2015); such constraints are especially interesting at the periphery of clusters and beyond, where the outskirts connect to cosmic filaments.

Measurements of metallicity in cluster outskirts are extremely challenging, and only exist for a handful of very nearby, bright, galaxy clusters. An excellent spectral resolution for diffuse sources is necessary for a reliable determination of the equivalent widths of faint emission lines (as demonstrated by Hitomi Collaboration, 2017). While the spectrometers on *XRISM*/Resolve and the *Athena*/X-IFU will undoubtedly reveal invaluable information regarding the chemical enrichment pattern in the cores of galaxy clusters and groups across cosmic time, the combination of high-resolution spectroscopy and a very large grasp offered by the proposed Cosmic Web Explorer is required to probe the metal abundance ratios in the outskirts of these halos, which span many square degrees on the sky, and give a definitive answer to the question: **what is the recipe for distributing the building blocks of life throughout the bulk of intergalactic space?** As shown in Figure 2, lines from both O (predominantly contributed by core-collapse supernovae) and Fe (primarily a SN Ia product) can be detected even for surface brightness levels expected far beyond r_{200c} , allowing us to determine how different enrichment sources contributed to the metal budget the region of ongoing virialization at the edge of the clusters' X-ray halos.

2.1.5 Non-equilibrium phenomena in cluster outskirts

Besides thermal, kinematic and chemical properties of the ICM, the cluster formation process gives rise to a variety of still poorly understood *plasma physics* across a wide range of scales. For example, in the extremely low-density regions in cluster outskirts, the Coulomb collision time of electrons and protons becomes longer than the age of the Universe (e.g. Rudd & Nagai, 2009; Avestruz et al., 2015). **How do electrons get heated in cluster outskirts? What is the role of magnetic fields in mediating the equilibration between different particle species in the plasma? Does the ideal fluid approximation, which is often employed in numerical simulations of large-scale structure formation, break down? If so, at what point?**

Hitomi offered us a first glimpse into the power of high-resolution spectroscopy to probe deviations from the collisional ionization approximation (Hitomi Collaboration et al., 2018a), and measure the ion temperature independently of the electron temperature (Hitomi Collaboration et al., 2018b) in the bright core of the Perseus Cluster. These diagnostic tools require excellent spectral resolution and a very large number of spectral counts which, for the faint and very extended cluster outskirts, can only be obtained with the proposed Cosmic Web Explorer.

Detecting the signature of non-thermal phenomena in cluster outskirts has the potential to provide a view of out-of-equilibrium plasma conditions, where relativistic particles can be accelerated in a so-far unexplored plasma regime (e.g. Bykov et al., 2019) and give rise to observed diffuse radio emission by interacting with diffuse magnetic fields (e.g. Brunetti & Jones, 2014). Key unknown quantities to understand how these processes proceed are the Mach number of accretion shocks, the exact thermodynamic structure of post-shock relaxation regions, as well as the degree of plasma collisionality here (e.g. Bykov et al., 2008; Brunetti & Lazarian, 2011) – quantities which the proposed mission is ideally equipped to probe. Combined with forthcoming constraints on the non-thermal phenomena of the universe from radio (e.g. LOFAR, MWA, ASKAP, MEERKAT and SKA; see discussion in § 4), **the Cosmic Web Explorer will allow us to connect the physics of the thermal and relativistic large-scale Universe in unprecedented detail.**

2.2 The circumgalactic medium as a driver of galaxy evolution

Most of the stars and metals in the Universe were formed in approximately Milky Way mass, $M_{\text{tot}} \approx 10^{12} M_{\odot}$, galaxies. The majority of baryons in these L^* galaxies reside in shock heated atmospheres with temperatures of millions of degrees, extending far beyond the stellar component. About half of the yet unseen warm-hot diffuse matter in the local Universe may lie in such extended galactic atmospheres (e.g. Fukugita et al., 1998; Kereš et al., 2005; Fukugita & Peebles, 2006). **Gaseous halos are inextricably linked to their host galaxies through a complex story of accretion, feedback, and continual recycling.** The energetic processes that define the state of gas in the CGM are the same ones that regulate stellar growth and create the diversity of today’s galaxy colors, star formation rates, and morphologies, spanning Hubble’s Tuning Fork Diagram.

How does matter cycle between galaxies and structures on larger scales? Our understanding of galaxy evolution is critically limited by our poor understanding of the cycling of baryons through the circumgalactic and intergalactic media. We are in the era when UV absorption studies, mainly focused on the OVI emission line doublet, but also probing many other metal ions with ionization potential energies < 10 Ryd, are dramatically increasing our knowledge of the CGM (e.g. Tumlinson et al., 2011; Werk et al., 2016). These observations are shifting focus to the CGM as one of the most crucial probes of galaxy evolution. Despite the large interest generated by these observations in the community, we are still unclear about the nature of the absorbing gas: is it hot collisionally ionized gas (Oppenheimer et al., 2016), warm photo-ionized gas (Stern et al., 2016; Oppenheimer et al., 2018), or conductive layers at the interface between different media (Armillotta et al., 2017)? Determining which of these scenarios is correct would have important implications for our understanding of the multiphase nature of the CGM and the cycle of baryons around galaxies (McQuinn & Werk, 2018). This goal, however, cannot be achieved based only on the pencil-beam views offered by absorption studies and, most importantly, without the more comprehensive view based on the study of higher ionization states of oxygen and other metals.

The bulk of the gas-phase oxygen in the CGM is expected to be in the form of OVII and OVIII (Figure 3, lower left panel), which both have strong soft X-ray emission line multiplets. Modern simulations which are able to reproduce the basic optical galaxy properties (Figure 3, top panel), such as Illustris, IllustrisTNG, and EAGLE, differ in their predictions of the OVII and OVIII radial profiles by many orders of magnitude, particularly for lower-mass galaxies (below $\approx 10^{12} M_{\odot}$, Figure 3, lower right). Direct mapping of the intensity, as well as line of sight velocities and velocity dispersions of these lines will provide the robust and comprehensive understanding of the CGM required to constrain models of galaxy formation and evolution.

The hot atmosphere of our own Milky Way Galaxy contains about $2.5 \times 10^{10} M_{\odot}$ of gas (Bland-Hawthorn & Gerhard, 2016), and the baryonic mass fraction within the virial radius is only $\approx 6\%$,

which falls well short of the Universal cosmic value of 16%. Some kind of violent activity likely caused our Galaxy to lose a large part of its hot atmosphere.

The Galactic centre shows abundant evidence for such violent activity: gamma-ray observations have identified giant cavities filled with relativistic plasma – called Fermi bubbles – on both sides of the Galactic plane, which indicate that our Galactic centre has recently released large amounts of energy. Recently, Ponti et al. (2019) reported the discovery of prominent X-ray structures above and below the plane. These “Galactic Centre Chimneys” may constitute a channel through which energy and mass, injected at the Galactic centre, are transported to the base of the Fermi bubbles. These events may lead to the heating, enrichment, but also to the partial loss of the Galactic atmosphere. High resolution X-ray spectroscopy with *XRISM* and *Athena* will significantly improve our knowledge of the temperature structure and metallicity of Milky Way’s atmosphere. However, the spectral resolution at low energies (corresponding to > 1000 km/s for the X-IFU) will not be sufficient to constrain the velocity structure, and the small FoV of these instruments will only allow us to obtain pieces of the puzzle - not a contiguous map over a wide field. **An X-ray observatory with a large field of view and high spectral resolution in the soft band ($R = 2000$ at 0.6 keV) will revolutionize how we view the dynamical interaction between the hot atmosphere of our own Galaxy, outflows and jets from the supermassive black hole SgrA* at its center, and stellar feedback.**

Studies of other spiral galaxies with *Chandra* and *XMM-Newton* also find less baryonic mass in their atmospheres than expected. When the observed density profiles are extrapolated to the virial radius of these galaxies, more than 60–70% of the baryons appear to be missing (Anderson et al., 2016; Bogdán et al., 2017; Li et al., 2018). The atmospheres of at least some of these disk galaxies could be in an outflow state (Pellegrini et al., 2018). Bregman et al. (2018) show that the atmospheric density profiles of massive spirals need to be extrapolated out to $1.9\text{--}3 r_{200c}$ for their baryon to dark matter ratio to approach the cosmic value. Even with long, \sim Ms observations, *Athena* will only probe the central regions of $\sim L^*$ galaxies (out to $0.4 R_{\text{virial}}$, Kaastra et al., 2013), and can not resolve their line widths and shifts, demonstrating the importance of a future instrument with much higher throughput and improved spectral resolution at soft X-ray energies.

The question of the baryon content of galactic atmospheres is further complicated by our lack of knowledge about their metallicity. Today, we only have reliable constraints on the chemical composition of hot atmospheres surrounding massive ellipticals, which have metallicities approaching the Solar value (Mernier et al., 2018b). In general, their metal abundances peak in their centres and flatten out at $\approx 0.2 - 0.3$ Solar at larger radii (Mernier et al., 2018a). Whether the same is true for lower-mass galaxies is still unknown. This is particularly important because these low-mass halos are increasingly dominated by stellar feedback, of which metals are faithful tracers.

The CGM provides the fuel for galaxy formation and is fed by both cosmological accretion and feedback processes. L^* spiral galaxies that are forming stars at the rate of our Milky Way ($\approx 2 M_{\odot} \text{ yr}^{-1}$) would consume the available molecular gas in their discs in about 10^9 years. To maintain their star-forming galactic discs, they have to be fed continuously by molecular gas from outside (Fraternali & Tomassetti, 2012). Thermal instabilities in their hot atmospheres, leading to a “rain” onto the galactic disc, would be able to provide plenty of fuel to maintain the star formation in spirals for $\approx 10^{10}$ years. During this phase of galaxy evolution, the hot atmosphere is not only a source of mass for the galaxy, but necessarily also of angular momentum: otherwise, galaxy discs would inevitably shrink with time, opposite to observations (van der Wel et al., 2014). While this important aspect has been the subject of recent theoretical studies (Pezzulli et al., 2017; Oppenheimer, 2018), a robust observational determination of the rotation of hot atmospheres is close to impossible with the current instrumentation (Hodges-Kluck et al., 2016), further highlighting the need for the high spectral resolution mission proposed here.

Thermally unstable cooling from the hot galactic atmospheres is also relevant in early-type galaxies where it likely feeds the central supermassive black hole. When gas from the hot halo

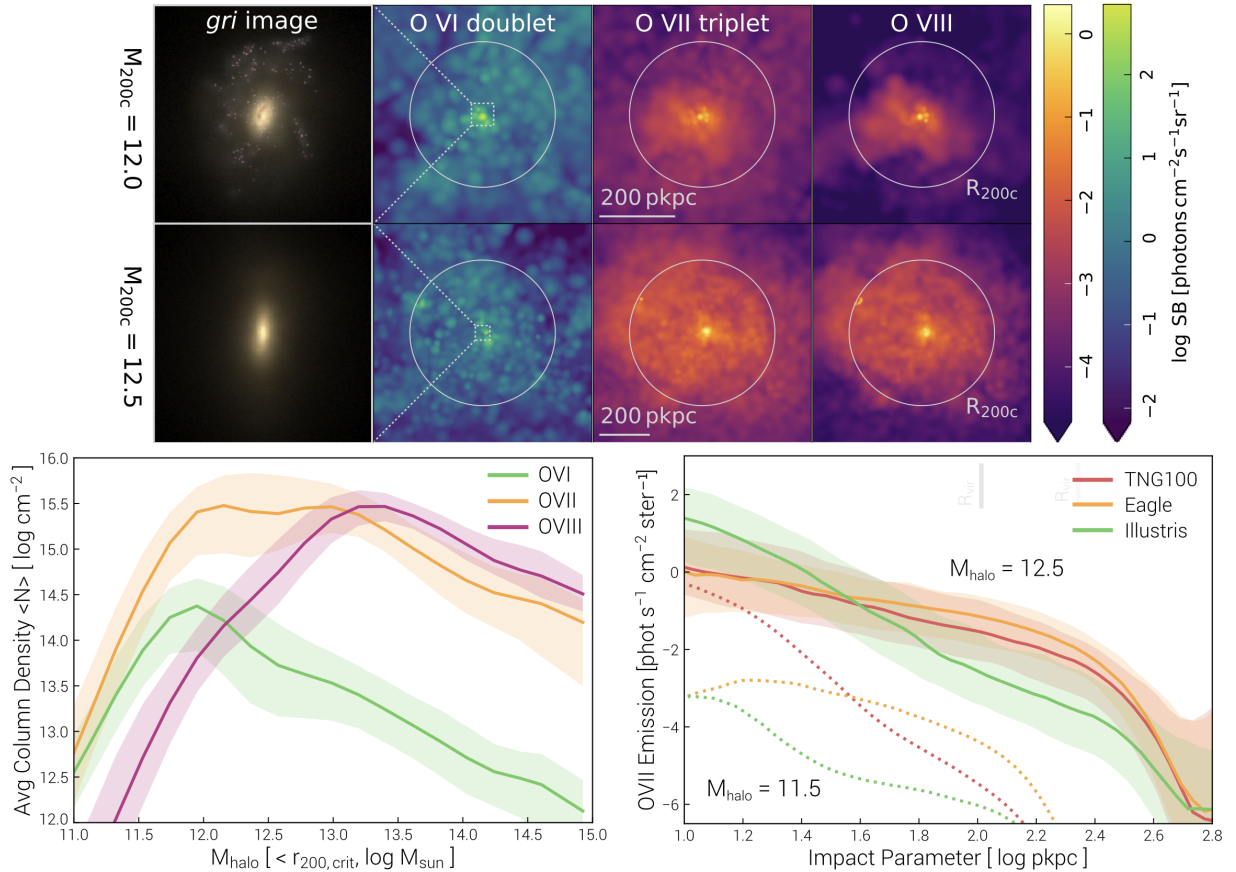


Figure 3: Emission signatures from diffuse baryons in the CGM as predicted by three current large-volume cosmological hydrodynamical simulations: Illustris (Vogelsberger et al., 2014), EAGLE (Schaye et al., 2015), and IllustrisTNG (Pillepich et al., 2018b). These three simulations invoke different galaxy formation physics and include a diverse range of black hole feedback models. (Top:) Predicted surface brightness maps in the OVI, OVII, and OVIII emission lines for two halos of different mass chosen from the EAGLE simulations, and their connection to the central galaxy at the heart of each halo. (Lower left:) OVII and OVIII ions dominate in abundance over the commonly observed UV-wavelength OVI ion, even in the CGM of Milky Way mass galaxies (Nelson et al., 2018). (Lower right:) Different models predict a diversity of signatures for the thermal, kinetic, and ionization properties of the hot baryonic phase, particularly for lower-mass Milky Way and group-size halos, regimes largely unconstrained by current X-ray observational facilities.

condenses into cooler clouds that “precipitate” toward the center (Gaspari et al., 2013; Voit et al., 2015; McNamara et al., 2016), the accretion rate can rise by orders of magnitude, triggering a feedback response by the AGN which heats the gas and balances its cooling. This closes the feedback loop needed to maintain a very delicate equilibrium, regulating the star formation rate and ensuring the co-evolution of its SMBH and host galaxy.

The detailed physics of the development of cooling instabilities and multi-phase gas, which is key for the formation of galaxies, stars and planets, is not understood and would require spatially resolved X-ray spectra providing detailed knowledge of the dynamics, temperature structure, and chemical composition of the hot atmospheric gas. Because the dense cooling gas and the hot phase need to be close to pressure equilibrium, information on the hot phase is crucial to understand the properties of the cooling gas observed at other wavelengths. **To measure the level of turbulence, which may play a key role in the formation of thermal instabilities, and to quantify the velocities and chemical make-up of both inflows and outflows close to the virial radii of galaxies, thus providing a final answer regarding feedback and the circulation of baryons in and out of L^* halos, several improvements with respect to the capabilities**

of *Athena* are essential.

The measurement of gas velocities of around 100 km/s, as well as the detection of very faint soft X-ray emission in the outskirts of galaxies will require a high spectral resolution of $E/\Delta E = 2000$ at 0.6 keV, a very large photon collecting area, and a low detector background. All these must be achieved while (at minimum) maintaining *Athena*'s spatial resolution of ~ 5 arcsec, which allows us to separate the emission of the inner CGM from that of the ISM and WHIM on scales of ~ 10 kpc at $z=0.1$. A large FoV further offers the benefit of potentially probing several galaxy halos within a single observation, and increasing the studied sample size considerably. A future observatory with these capabilities will revolutionize our picture of the CGM and its link to galaxy evolution.

2.3 The role of galaxy groups in structure formation

Groups of galaxies (defined as objects with $10^{13} < M_{500} < 10^{14} M_{\odot}$) bridge the mass spectrum between galaxies and galaxy clusters. As such, they are critical systems for understanding the process of structure formation, the dynamical assembly of baryons in dark matter halos, and the complex physics that affects both the gas and the stellar components.

Groups of galaxies are known to host a significant fraction of the number of galaxies in the Universe (e.g. Eke et al., 2006), and unlike galaxy clusters they form also in the filaments of the cosmic web rather than only in the nodes (e.g. Tempel et al., 2014). Modern hydrodynamical simulations (e.g. Le Brun et al., 2014; Planelles et al., 2014; Truong et al., 2018) show that the depletion of baryons in halos with $M_{500} < 2 \times 10^{14} M_{\odot}$ due to complex baryonic physics (e.g. cooling, galactic winds, AGN feedback) plays an important role in explaining the breakdown in self-similarity, wherein the $L_X - T_X$ relation shows a slope steeper than the expected value of 2 (~ 3 , Pratt et al., 2009; Maughan et al., 2012) at the cluster scale, further steepening at the group scale (e.g. Osmond & Ponman, 2004; Sun, 2012).

Understanding how the gas content of the outskirts of galaxy groups is affected by non-gravitational processes is needed to calibrate the baryonic effects on the matter power spectrum (e.g. Hearin et al., 2012; van Daalen & Schaye, 2015; van Daalen et al., 2019) and is an important ingredient for deriving cosmological constraints from ESA's upcoming Euclid mission.

In the coming years, *eROSITA* (Merloni et al., 2012) is expected to find over 10^5 massive halos through their X-ray emission, a large fraction of them groups with masses below $10^{14} M_{\odot}$ (Borm et al., 2014), enabling cluster cosmology with an unprecedented statistical sample (e.g. Pillepich et al., 2018a). *Athena* (Nandra et al., 2013) will provide tighter constraints on the scaling relations and radial thermodynamic profiles of these objects (Ettori et al., 2013; Pointecouteau et al., 2013).

However, studies with existing or approved missions, such as *eROSITA* and *Athena*, will be typically limited to the inner parts of galaxy groups. The mission envisaged here will combine both advantages, large grasp and high spectral resolution, thereby enabling a quantum leap in our study of the outskirts of galaxy groups. In particular, the Cosmic Web Explorer will address better than ever before fundamental questions such as: **What is the baryon fraction out to r_{200c} for the general population of galaxy groups as a function of radius and cosmic time? What are the roles of AGN feedback and non-thermal pressure in breaking self-similarity at the group scales? How does this baryonic physics affect the matter power spectrum on non-linear scales?**

2.4 Filling the bridges, and emptying the voids, of the large-scale structure

Most of the baryons in the local Universe are expected to be distributed along the filamentary structures that compose the backbones of the "Cosmic Web". Studies of UV-absorption lines with FUSE and HST-COS (Shull et al., 2014) have probed the coldest fraction of these baryons. Hydrodynamical simulations (e.g. Cen & Ostriker, 2006) show instead that, much like for the CGM,

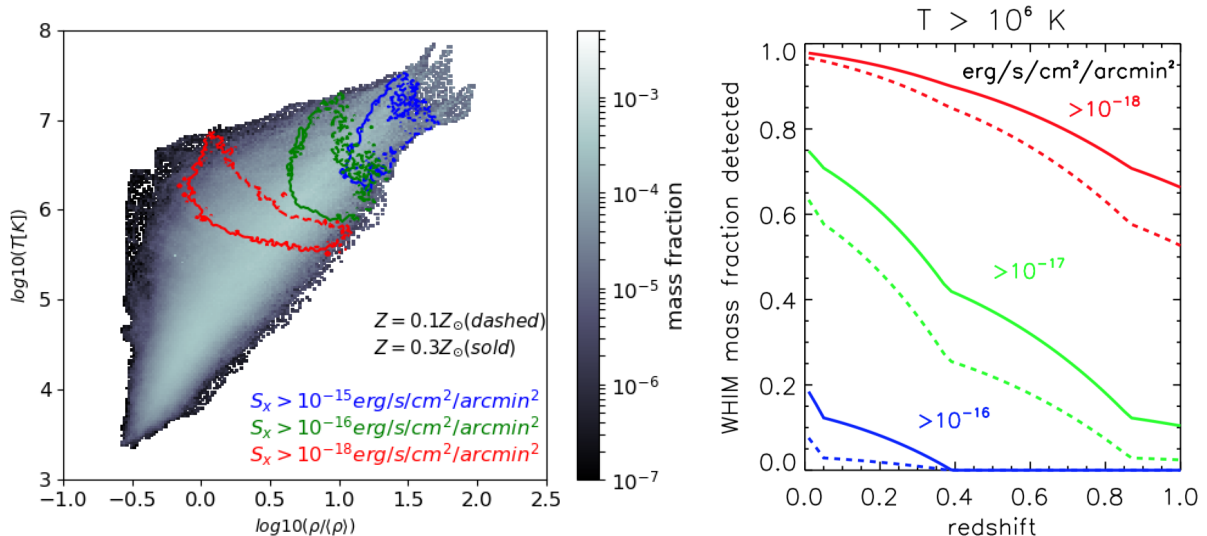


Figure 4: (Left) Phase diagram of the gas in a comoving 85 Mpc^3 volume, simulated using 1024^3 cells with the ENZO code (Bryan et al., 2014) and including the effect of magnetic fields, radiative cooling, star formation, supermassive black holes, and of the thermal feedback from star-forming regions and AGN as detailed in Vazza et al. (2017). Lines indicate the sensitivity required to observe it. (Right) Distribution of the mass fraction of the gas at $T > 10^6 \text{ K}$ that is expected to be resolved, as function of redshift, at different cuts in surface brightness in the 0.3–2 keV band, and for different metallicities.

the hotter phase is the dominant one (i.e. $T > 10^{5.5} \text{ K}$), and it can be detected preferentially through highly ionized C, N, O, Ne, and Fe ions in X-rays.

Our understanding of how the growth of cosmic structures has developed requires that such baryons must have been processed by strong shocks at least once during their lifetime, where their infall kinetic energy has been mostly dissipated into thermal energy (e.g. Sunyaev & Zeldovich, 1972; Bykov et al., 2008, 2019). While there are hopes to detect at least the “tip of the iceberg” synchrotron signature of relativistic electrons accelerated by accretion shocks with the new generation of radio telescopes, the challenge of detecting such strong shocks (which are a pillar of our understanding of the WHIM picture) can only be tackled by finally imaging diffuse gas flows associated with $\sim 10^6 - 10^7 \text{ K}$ post-shock temperatures.

Away from higher-density regions that are being actively heated and stirred by complex stellar and AGN feedback, the truly diffuse, extended WHIM is a unique probe of structure formation processes and chemical enrichment history. Through both cosmic accretion and metal dispersion by feedback, the physical properties of the WHIM are a direct consequence of the interplay between the intergalactic medium (IGM), galaxies, and the action of gravity on much larger scales.

What is the structure of the Cosmic Web? To date, only few reliable detections of the WHIM in absorption have been reported, using very long observations of bright, distant quasars (Nicastro et al., 2018); the list is equally short for individual detections of LSS filaments in emission, which have typically been identified as they connect to the outskirts of massive galaxy clusters (see Section 2.1.2). The *Athena*/X-IFU will probe ~ 200 of the strongest OVII absorbers associated with large-scale structure filaments, with typical properties expected to account for around 20% of the WHIM baryon mass. In a few cases, the corresponding emission from the WHIM will also be detected. Given *Athena*’s spectral resolution in the soft X-ray band, such studies will be focused on the detection of the WHIM; its kinematics (and thus energetics) and, to a large part, its temperature and metallicity, will remain unexplored. **We therefore need a mission with new capabilities that, in addition to spatially mapping the vast majority of the X-ray emitting cosmic web, will also routinely provide information about its detailed physical properties.**

Figure 4 shows that a surface brightness sensitivity of $\sim S_x \sim 10^{-18} \text{ erg/s/cm}^2/\text{arcmin}^2$ in

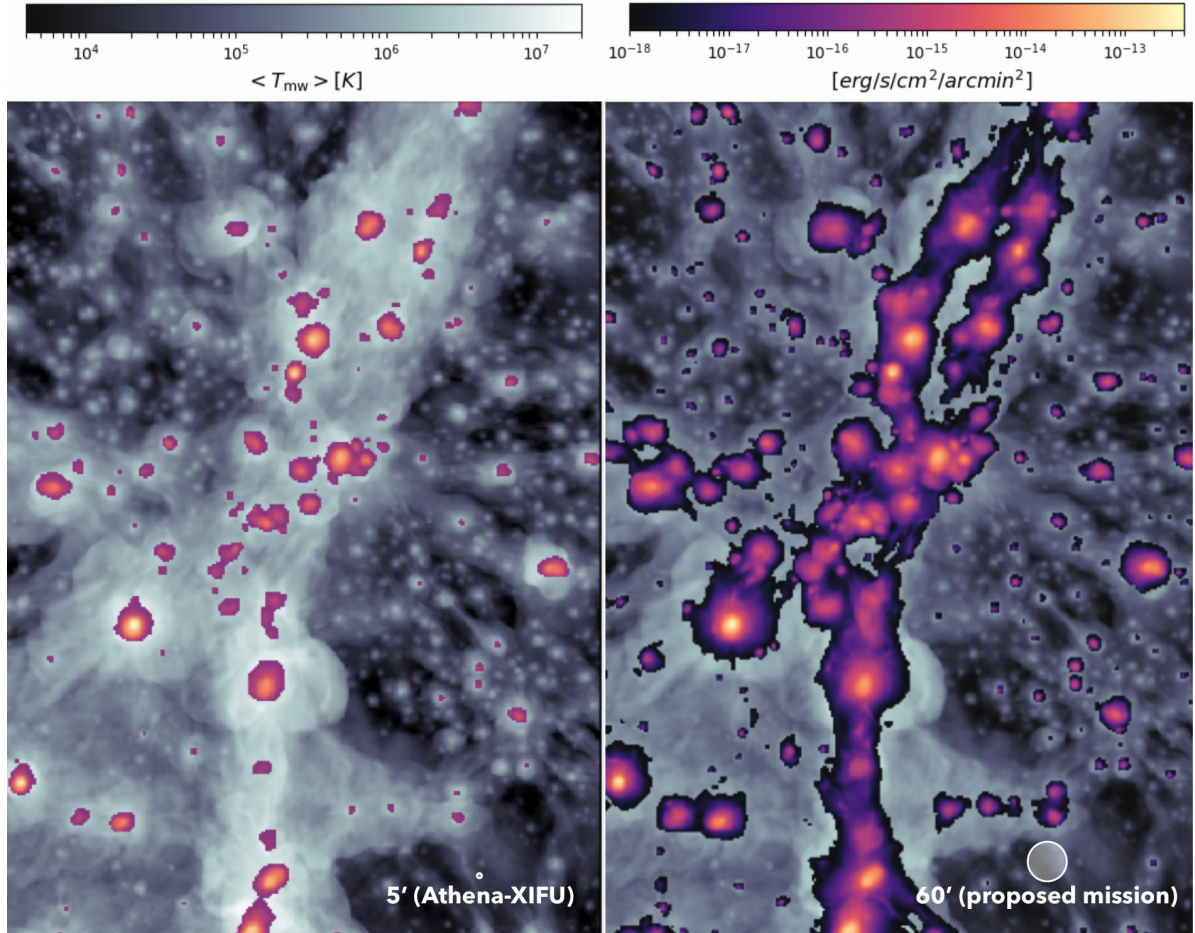


Figure 5: Projected mass-weighted gas temperature and detectable X-ray emission in the 0.3–2 keV energy band at $z \approx 0.05$ extracted from a cosmological hydrodynamical simulation (Vazza et al., 2019). Two different limits in surface brightness are used: (right) $\sim 1 \times 10^{-18} \text{ erg s}^{-1} \text{ cm}^{-2} \text{ arcmin}^{-2}$, which is the target for the proposed mission; (left) $\sim 5 \times 10^{-16} \text{ erg s}^{-1} \text{ cm}^{-2} \text{ arcmin}^{-2}$, which should be reachable by *Athena* for a similar investment in observing time, factoring in the difference in grasp and instrumental background. Each panel is $\sim 15^\circ \times 11^\circ$ across, about 10% of the area that can be surveyed at this depth in 5 years with the proposed mission. The expected FoV for the *Athena*-XIFU (5 arcmin) and the Cosmic Web Explorer (1 deg) are shown in the lower right corner of both panels.

the 0.3–2.0 keV band is sufficient to **detect all of the diffuse baryons with a temperature $T > 10^6 \text{ K}$, and probe overdensities of $\rho / \langle \rho \rangle \sim 1$** . For a WHIM component in collisional ionization equilibrium with $kT \sim 0.2 \text{ keV}$ and a metallicity similar to the cluster outskirts (0.3 Solar), and modeling the foreground and background contributions as shown in Figure 2, we find that **an exposure time of 50 ks with the proposed mission would allow us to detect at least two emission lines (OVIII and one line in the OVII triplet) each with a significance greater than 5σ per 1000 arcmin² extraction area. With a 5-year mission and given the observing efficiency in low-Earth orbit (LEO), 1600 square degrees can be surveyed at this depth**. Deeper observations can be used in the case that the metallicity and ionization state of the WHIM are different than these assumptions⁴. Figure 5 shows the dramatic improvement in our ability to map the WHIM using the proposed mission compared the *Athena*/X-IFU, for a comparable investment of observing time.

The expected signal is much weaker than the cosmic foregrounds and backgrounds. Priors on

⁴Observations of 1 Ms can probe OVIII emission down to a limiting flux of $6 \times 10^{-12} \text{ photons/s/cm}^2/\text{arcmin}^2$.

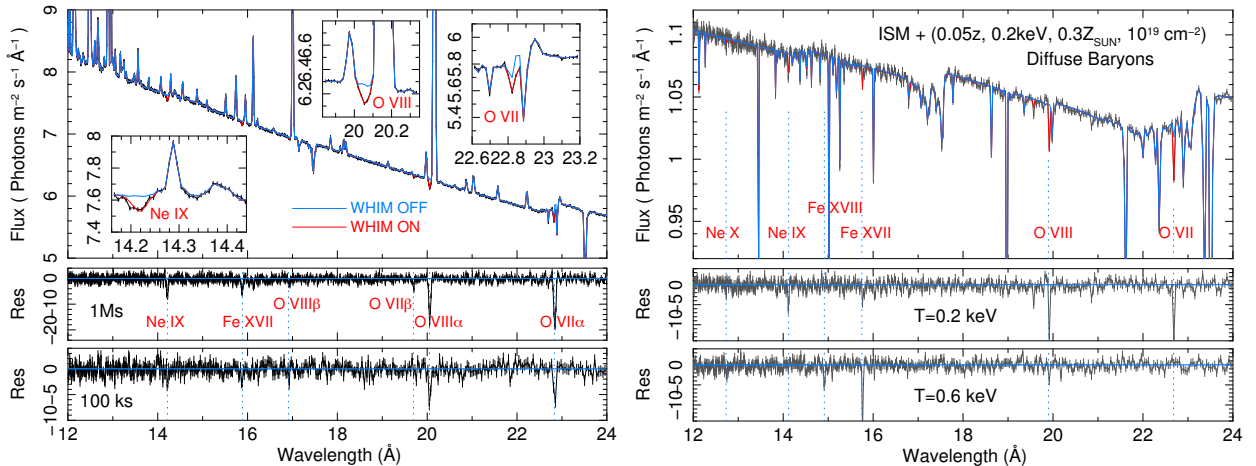


Figure 6: Simulations of faint, diffuse baryons that can be detected in absorption by the proposed mission. Left: an observation of a WHIM filament with $kT=0.2$ keV, $Z=0.3$ Solar, and $n_H=10^{19}$ cm^{-2} , assumed to exist in projection in front of the cool core of A1795 at $z=0.06$, with a velocity difference of -1500 km/s from the cluster core. Both emission lines from the cool core and absorption lines from the WHIM can be clearly studied even for a relatively short 100 ks exposure (bottom panel residuals). Right: more than 100 AGN with fluxes above 10^{-14} ergs/s/ cm^2 are expected to be found within 1 square degree. Shown is a simulated, stacked spectrum of these AGN with an exposure of 1 Ms, with the same properties for the absorbing gas as in the left panel. A shorter 100 ks observation (not shown) would already result in a highly significant detection ($\Delta C_{\text{stat}} \sim 50-80$). For an absorber with a temperature of 0.6 keV (representative of the gas immediately inside the accretion shock of a massive galaxy cluster), the residuals for $N_H = 5 \times 10^{19}$ cm^{-2} absorbed by the same CXB are shown in the bottom right panel. Column densities below 1×10^{19} cm^{-2} at $kT = 0.6$ keV can be reached in absorption against bright blazars.

the spectral shape of the WHIM, together with detailed modeling of the foregrounds and noise, will be of paramount importance to extract the information we are searching for. This is a challenging task, but one where we can build upon improvements in spectral models of emission from our own Galaxy driven by XRISM *Athena*, as well as the experience with data analysis techniques from cosmic microwave background (CMB) and gravitational wave science.

Simultaneous emission and absorption spectroscopy will allow for direct, model-independent measurements of the gas density, length scale, ionization balance, excitation mechanism (or gas temperature), and element abundance. Absorption studies along independent lines of sight, numerous enough to minimize the impact of cosmic variance, can set strong constraints on the WHIM properties. What makes the proposed mission unusually powerful compared to a grating spectrometer is that, in addition to mapping faint emission over large areas of the sky, **column densities as low as $N_H \sim 10^{19}$ cm^{-2} can be probed in absorption against the ubiquitous cosmic X-ray background**, by stacking faint point sources detected in the field (see right panel of Fig. 6). We therefore no longer have to rely on the serendipitous existence of a bright AGN within the region of interest to probe it. Moreover, only a non-dispersive X-ray spectrometer can use the diffuse ICM as a backlight for absorption studies. Clusters are among the brightest X-ray sources and reside at the nodes of the cosmic web; thus cluster sight lines are likely to pass through the densest regions of the WHIM. The proposed mission will study in great detail the absorption spectra from all WHIM filaments lying in projection in front of galaxy cluster cores (see left panel of Fig. 6).

Models based on hydrodynamical simulations (see e.g. Borgani et al., 2004) predict that WHIM filaments show a characteristic signal at angles of a few arcminutes that can be used to disentangle the WHIM from other components of the unresolved X-ray background (see Roncarelli et al., 2006; Hickox & Markevitch, 2007), with uncertainties related to its metal composition (Ursino et al., 2010; Cen & Chisari, 2011; Roncarelli et al., 2012), and an associated high cosmic variance (see e.g. Ursino et al., 2014). This emission can be resolved as a signal in the angular auto-correlation function (or its analogue in the Fourier space, the power spectrum) on arcminute scales, although

the peak in the signal will move to smaller angles for contributors at higher redshifts. Once the rich structure of the cosmic web is also resolved in redshift, higher order statistics, such as the 3-point correlation function and tools from graph theory (e.g. Naidoo et al., 2019), can be applied for robust cosmological parameter inference using the densest structures. Cross-correlations with other plausible signposts of the cosmic filaments, such as galaxy luminosity density (see, e.g., Nevalainen et al., 2015) and diffuse inverse Compton scattering of the CMB photons on the WHIM in mm bands (see, e.g., Tanimura et al., 2019) will enhance the signal associated with the WHIM emission. Ursino et al. (2014) show that the cross-correlation of the WHIM signal in the soft (e.g. 0.4–0.6 keV) X-ray and SZ maps is dominated by the gas within $z < 1.5$ and peaks at scales of a few arcmin (multipole $l \sim 10000$). Combining radio and X-ray observations will also allow us to detect the cosmic web illuminated by structure formation shocks (Vazza et al., 2019). Gas “bridges” tracing the leading merger axis between clusters in an early merging stage are boosted both in radio and X-ray emission, compared to the more typical conditions found in cluster outskirts. These boosted emission regions should be already visible with existing radio instruments (e.g. LOFAR; see Govoni et al., 2019), and can be studied in X-rays with *Athena*. In the future, the increased sensitivity of the SKA, together with the improved capabilities of the proposed Cosmic Web Explorer, can push this type of joint exploration towards fainter and more representative WHIM filaments.

A role complementary to the filamentary structure of the cosmic web is played by the cosmic voids. Devoid of matter by definition, they are dark energy-dominated objects, and are particularly sensitive to neutrinos (and all diffuse components) since the mass fraction of neutrinos with respect to CDM is higher in voids than in high density regions. The evolution of voids is ruled by the joint action of gravitational attraction, that empties voids by pushing material towards their boundaries, and the expansion of the Universe, that also enlarges voids by diluting the space between galaxies. For these reasons (see, e.g., Pisani et al., 2019), observables such as number, size, shape, distribution and clustering of cosmic voids are powerful probes of the properties of the dark energy and neutrinos.

Tomographic observations of the soft X-ray emission from contiguous patches of the sky will allow the reconstruction, both directly and, at higher statistical significance, with auto-correlation function techniques, of the distribution of the WHIM at $T > 10^6$ K in different redshift bins (see Fig. 4). The combination of the signal on the sky at various redshifts will permit a first 3D mapping of the filaments (and relative voids) containing most of the elusive fraction of the missing baryonic mass.

3 Mission concept

3.1 Overview

The science questions described above can be answered with a mission providing the necessary combination of throughput, grasp, angular resolution, spectral resolution, and low and stable detector background. The basic mission concept is thus an L-class, large effective area X-ray telescope with a large field of view, focusing on an X-ray Integral Field Unit, and placed in Low-Earth orbit. Table 1 lists the driving scientific goals and associated mission requirements. The envisioned improvements compared to the *Athena* X-IFU are shown in Figure 7.

A small fraction of the science theme proposed here, namely probing the CGM, WHIM, and cluster outskirts only along selected sightlines towards bright background AGN, can be covered by an ESA Medium-Class mission based on dispersive technology spectrometers (see the White Paper by Nicastro, Kaastra et al. 2019 submitted in response to this call).

Table 1: Driving scientific goals behind each of the mission requirements. Implicitly, this also shows which science cases would be most affected if any of the proposed capabilities were reduced to achieve a smaller mission profile.

Parameter	Value	Science driver
Field of view	1 square degree	Mapping the connection between galaxy clusters and the large-scale structure; surveying cosmic web filaments; cross-correlation with galaxy distribution, weak lensing maps, SZ surveys over a wide area. Athena XIFU will have a diameter of 5 arcmin allowing detailed study of the gas kinematics in clusters only along pre-selected azimuthal sectors.
Angular resolution (90% enclosed energy fraction)	$\approx 5''$	Resolving structure in the circum-galactic medium; separating galaxy halos from the truly diffuse LSS filaments; removing contamination from point sources to a sufficient depth to enable the study of very faint diffuse emission. Athena's PSF will be comparable.
On-axis effective area	$\approx 10 \text{ m}^2 @ 1 \text{ keV}$	Detection and mapping of cosmic web filaments at low overdensities. Athena will have an effective area a factor of ~ 7 lower at 1 keV.
Energy band	0.1–3 keV	Studies of the chemical composition from C to Ni, up to and including K-shell lines of Si. Athena will be sensitive to energies up to $\sim 10 \text{ keV}$ that are not needed for the scientific case of the Cosmic Web.
On-axis sensitivity	$10^{-18} \text{ erg cm}^{-2} \text{ s}^{-1} \text{ arcmin}^{-2}$	Detecting and characterizing the cosmic large scale structure in emission at $T > 10^6 \text{ K}$. The combination of effective area and background reproducibility allows Athena to reach a surface brightness limit of a few times $10^{-16} \text{ erg/s/cm}^2/\text{arcmin}^2$ in the 0.5–2 keV band (see for a comparison Fig. 5).
Spectral resolution	$E/\Delta E = 2000$ at 0.6 keV	Measuring kinematics of the CGM. Efficiently detecting absorption lines for low column densities. Separating the expected signal from the Milky Way halo emission. Athena X-IFU will reach a resolving power of a few hundreds in the soft band.
Detector background	$\leq 1.5 \times 10^{-4} \text{ cts s}^{-1} \text{ keV}^{-1} \text{ arcmin}^{-2}$	Constraining the electron number density in faint, diffuse plasma from the bremsstrahlung continuum. Efficiently detecting faint emission lines against the continuum level. Athena X-IFU will have a nominal internal background of $\sim 5 \times 10^{-3} \text{ cts s}^{-1} \text{ cm}^{-2} \text{ keV}^{-1}$, corresponding to $\sim 6.1 \times 10^{-4} \text{ cts s}^{-1} \text{ keV}^{-1} \text{ arcmin}^{-2}$ for a 12m focal length.
Mission duration	5 years	To cover ~ 1600 square degrees with deep observations ($\sim 50 \text{ ks}$), given observing efficiency in LEO. Athena's nominal duration will be 4 years.

3.2 Mirror payload

In the conceptual design of the mirror module system, we assume segmented glass foils as a baseline technology, because glass can be shaped to high accuracy and low roughness. Glass foils have a low density (2.3 g/cm^3) and can be manufactured down to a 0.2 mm thickness, based on the experience

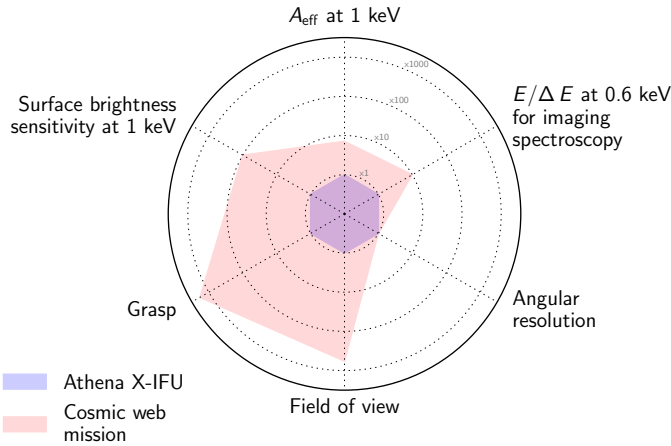


Figure 7: Enhancements in the capabilities of the proposed Cosmic Web Explorer with respect to the *Athena* X-IFU. Each dotted circle represents an order of magnitude increase. The substantial leap in grasp, coupled with the considerable improvement in spectral resolving power at low energies and the low detector background, lead to the significant advancement in surface brightness sensitivity required for the science theme.

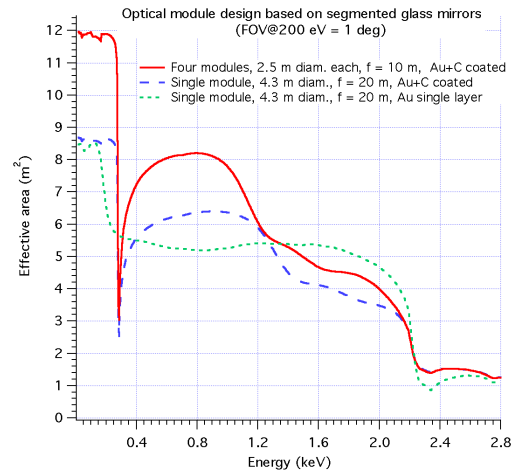


Figure 8: Effective area expectations. The solution based on four identical modules and an Au+C coating enables a considerable performance gain.

matured with NuSTAR (Harrison et al., 2013). This enables the minimization of obstructions and of the mirror module mass.

The initial design foresees the determination of the mirror module diameters and the focal length, aiming at reaching an effective area close to 10 m². To enhance the effective area at low energies, it is important to mitigate the photoelectric absorption by using a coating of amorphous carbon (Pareschi et al., 2004; Cotroneo et al., 2007). Here, we suggest as a guideline two different possible solutions, based on segmented glass shells and an Au+C coating. Alternative coatings such as Ir+C or Ir+SiC, or the use of various coatings for different mirror shells, can be optimized as the design is developed in more detail. Also, the current design assumes a Wolter-I mirror profile. To minimize off-axis degradation of the point spread function (PSF), Wolter-Schwarzschild or polynomial designs (Conconi & Campana, 2001) should be investigated at a more advanced stage of the mission definition.

Solution 1: single mirror module, 20 m focal length The first possible option is represented by 310 coaxial shells, with focal lengths of 20 m and diameters ranging from 4.3 m down to 1.492 m. There is no relevant benefit in extending the series beyond these limits. The shells are kept as close as possible, in order to minimize the dead areas between shells, but at the same time ensuring a FOV (50% vignetting function) of 1 deg in diameter. The mirror thickness is fixed at the value of 0.4 mm, and the total mirror mass is nearly 1000 kg.

Figure 8 shows the expected effective area with an Au+C coating, 150 nm Au and 30 nm C (red dashed line, assuming a further 10% of obstruction due to supporting structures). We can reach ~6 m² around the line energies of OVIII and Fe XVII. For comparison, the solution with bare gold is also shown (green, dotted line), with some gain around 2 keV, but at the expense of an effective area loss near 1 keV.

Solution 2: four mirror modules, 10 m focal length In order to shorten the focal length and reduce the detector background, while possibly increasing the effective area, we can divide the optical module into four identical sub-modules, each of them imaging onto a separate detector. If a fairing diameter of 6 m can be envisaged (commercial launch providers such as Blue Origin and

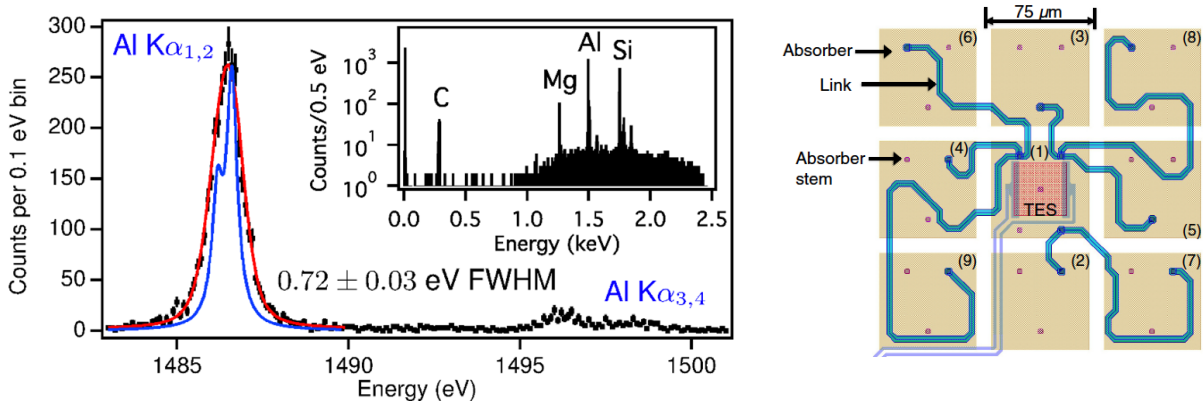


Figure 9: (Left:) Example measured spectrum of the Al $K\alpha$ complex. The blue curve is the intrinsic line shape, and the red curve is the best fit to the spectrum, demonstrating that a resolution of 0.7 eV is already achieved in the laboratory (Lee et al., 2015). (Right:) Schematic layout of a 9-pixel hydra (Smith et al., 2019). Multi-absorbers are connected to one TES with different thermal conductance (blue line), effectively reducing the number of TESs that need to be read out.

SpaceX plan to offer 7 m and 9 m fairings in the next few years), four identical mirror modules with a 2485 mm diameter can be accommodated. We consider a 10 m focal length and populate each module with decreasing diameters, keeping appropriate spacing between shells to preserve the geometric FOV. In this way, we can extend the series down to a 766 mm radius through 185 mirror shells. The total mirror mass now is ~ 1350 kg.

Figure 8 shows the comparison between the 1-module and the 4-module design. The 4-module concept enables higher effective area performances, with a considerable gain near 1 keV. An analytic computation (Spiga, 2011) of the off-axis area at 0.2 keV and 1 keV showed that the FOV is very close to 1 deg also with this design.

3.3 Detector payload

An integral field unit (IFU) provides the optimal combination of resolving power ($\Delta E/E \sim 2000$) and spatial resolution imaging ($\text{PSF} \leq 5''$) for the science theme. The resolving power requirement can be met by the use of a cryogenic X-ray microcalorimeter array. A number of technologies are under active development for the construction of such arrays, including metallic magnetic calorimeters (MMC, e.g. Kempf et al., 2018), metal insulator sensors (MIS, e.g. Sauvageot et al., 2016, 2018), and transition edge sensors (TES: for reviews, Irwin & Hilton, 2005; Ullom & Bennett, 2015).

As an example, the spectral performance of TES calorimeters can be described as

$$\Delta E \sim 2.45 \sqrt{\frac{k_B T^2 C}{\alpha}}, \text{ or } \Delta E \sim 2.45 \sqrt{k_B T E_{\text{Max}}}, \quad (1)$$

where k_B , T , C and α are the Boltzmann constant, detector temperature, heat capacity, thermistor sensitivity, respectively, and the saturation energy can be written as $E_{\text{Max}} = CT/\alpha$. Based on the scaling from the state-of-art performance of TES calorimeters, 0.5-0.7 eV @ 1.5 keV in laboratory conditions (Lee et al., 2015, and Figure 9, left), it is feasible to achieve $E/\Delta E \sim 2000$ assuming $E_{\text{Max}} \sim 0.6$ keV and $T \sim 60 - 70$ mK.

A large number of pixels would be needed to cover the wide FoV. Assuming a similar detector pixel size (pitch) as that of the *Athena* X-IFU ($275 \mu\text{m}^2$: ~ 5 arcsec 2), it would be necessary to have $3000 \times 60^2 / 5^2 \sim 4 \times 10^5$ pixels to cover a FoV with a diameter of one degree; ideally, this number could be further increased to avoid under-sampling the telescope's PSF. Such a quasi-mega-pixel

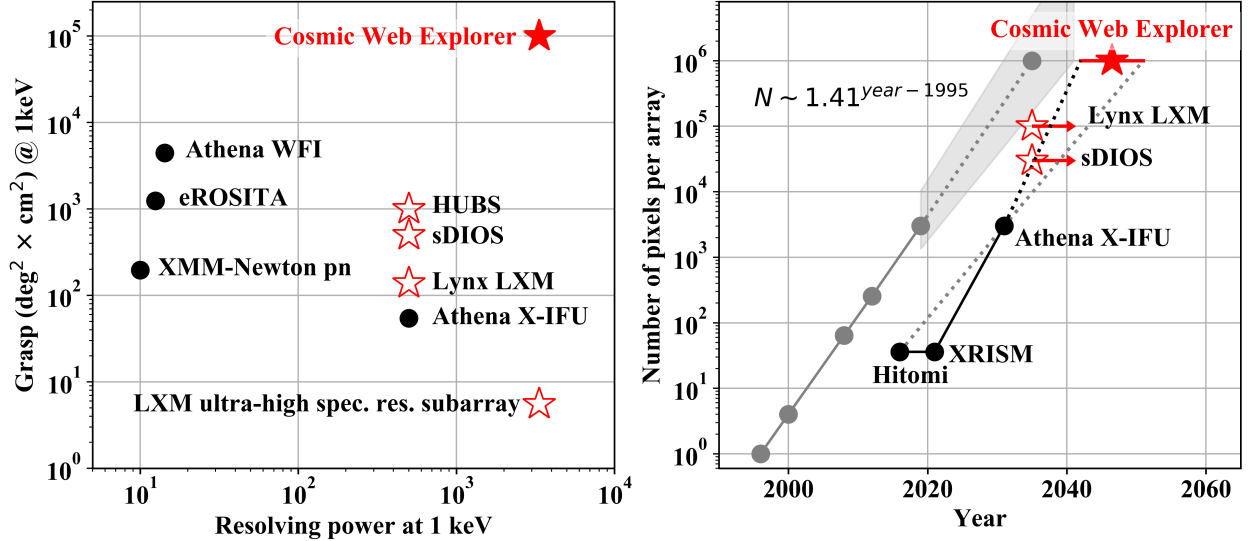


Figure 10: (Left) Grasp versus spectral resolution at 1 keV for selected operational/accepted (black circles) X-ray observatories and proposed mission concepts (red stars). (Right) Number of X-ray/gamma-ray calorimeters per instrument in laboratory environments (gray circles) vs. space (black circles for past or upcoming X-ray microcalorimeter missions at their respective launch year, red stars for a subset of mission concepts illustrating the expected future progress; horizontal red lines/arrows represent launch date uncertainties). The shaded gray area shows the extrapolation of a power-law function ($N \sim 1.41^{\text{year} - 1995}$) fit to the laboratory data, with conservative uncertainties.

array would represent a thousandfold increase in resolution elements compared to *Athena*, and even an order of magnitude more than that envisaged for the *Lynx* X-ray Surveyor, a high-energy flagship mission concept being considered for the NASA 2020 Astrophysics Decadal Survey (see Fig. 10, right). Several research and development (R&D) components will need to be addressed to make such a megapixel calorimeter array a reality. Some examples are shown below.

New multiplexing readout technology Due to the strict limit of available electrical and cooling power in space, the multiplexing readout technology is one of the key R&D items required for the proposed project. One of the most promising multiplexing technologies currently under development is the *Microwave SQUID multiplexer* (μ -wave MUX: Irwin & Lehnert, 2004; Mates et al., 2008). The μ -wave MUX consists of a number of superconducting resonators in the GHz range, each employing a unique resonance frequency, terminated by an inductance magnetically coupled to dissipationless rf-SQUID. This technology allows the readout of a number of TES pixels that is an order of magnitude larger than conventional multiplexing approaches.

Detector fabrication technology Even using μ -wave MUX technology, it can still be challenging to read out 10⁶ TES pixels. In this regard, multi-absorber TES (Fig. 9 right), in a so called *hydra* configuration, will increase the technological feasibility. Absorbers have different thermal conductance to TES. Therefore, even for the same incident photon energy, the response of each absorber is different. By using this difference of the response, the arrival information (i.e. which absorber recorded a photon hit) can be extracted. The *hydra* configuration effectively reduces the number of TESs.

Since the original concept of using a thermal detector as an X-ray spectrometer (Moseley et al., 1984) proposed about 35 years ago, we are now halfway to our goal leading up to the year 2050. Considering the progress made so far, we are confident that, building upon the advancements driven by the *Athena*/X-IFU instrument design, all technological developments are feasible with continuous effort.

4 Synergies in the context of astronomy into the 2050s

For the science questions described above, there is a strong synergy between the proposed mission and many other facilities, both ground- and space-based, that will be dedicated to exploring galaxy overdensities, dark matter, and the gas phase as tracers of the Cosmic Web structure, and span the entire spectral range from X-ray to radio.

The hot and warm phase of the Universe Beyond *eROSITA*, XRISM, and *Athena*, several mission concepts are under study. The Hot Universe Baryon Surveyor (HUBS⁵) and the Diffuse Intergalactic Oxygen Surveyor (Yamada et al., 2018, Super DIOS), with a much lower sensitivity and grasp and lower resolving power compared to that of the proposed mission (see Fig. 10, left), will pave the way for a deep exploration of the warm gas in the Cosmic Web over large areas of the sky. The Advanced X-ray Imaging Satellite (Mushotzky, 2018, AXIS) and the *Lynx* X-ray Surveyor (Gaskin et al., 2017) will provide a complementary, exquisite spatial resolution (down to 0.5 arcsec), allowing us to map substructure in the gas with very high detail.

In the coming two decades, projects such as CMB-S4 (Abazajian et al., 2019), the *Simons* Observatory (The Simons Observatory Collaboration et al., 2019), and *LiteBIRD* (Hazumi et al., 2019) will build up our knowledge of massive halos from the SZ effect and push the investigation of the millimetre CMB sky a step further. Beyond the 2030s, a high resolution, high sensitivity large millimetre telescope such as the AtLAST (Klaassen et al., 2019) and CMB-HD (Sehgal et al., 2019) concepts would bring opportunities that complement spectroscopic X-ray measurements. These features, generalised to a survey over a large area of the sky, would lead to a wealth of constraints on the thermodynamical properties (via the thermal and relativistic SZ effects), the peculiar motions (via the kinetic SZ effect) or the mass (via CMB lensing) of large scale structures. Such a mission concept is being proposed in the framework Voyage 2050 (Basu et al. 2019). The strong connection between X-ray and SZ for the physical characterisation of hot plasmas is already well established (Bulbul et al., 2019; Mroczkowski et al., 2019), meaning that these future SZ observatories offer crucial synergies with the mission proposed here. Both observables will provide a complementary view of the thermodynamics and kinematics of warm-hot plasmas in the CGM, ICM and WHIM out to the epoch of massive halo formation ($z \sim 2 - 3$).

The Large UV Optical Infrared Surveyor (LUVOIR) will provide another excellent complement to our proposed mission concept. LUVOIR's UV spectroscopy capabilities are uniquely poised to bring about a revolution in our understanding of gas flows, enrichment, and ultimately galaxy evolution on a wide range of cosmic scales (The LUVOIR Team, 2018). The combination of the cool-hot UV and warm-hot X-ray emission lines will deliver a comprehensive picture of the complex physical phases of the baryons filling the LSS. This will allow us to probe the composition and physical processes that define gaseous halos over the mass spectrum, delivering a transformative understanding of galaxy evolution, galaxy cluster physics, and gas within the Cosmic Web.

The light and the dark phase of the Universe In the next decades, several optical and IR telescopes will survey the distribution of galaxies and quasars over very large patches of the sky: *DESI*⁶ is set to start in the summer of 2020; *Euclid*⁷ will be launched in 2022; *LSST*⁸ will start a 10-year campaign at full regime in 2023, when *SPHEREX*⁹ will begin the first all-sky spectral survey between 0.75 and 5 μm . By 2050, all of these facilities will produce catalogues of tens of millions of galaxies and, through their overdensities and measured gravitational shear, will map the distribution of dark matter and stars in the LSS over most of the sky and out to the epoch of reionization, locating the regions where baryons in the hotter phase are expected to reside.

⁵<http://heat.tsinghua.edu.cn/hubs/en/index.html>

⁶<https://www.desi.lbl.gov>

⁷<https://www.euclid-ec.org/>

⁸<https://www.lsst.org/>

⁹<http://spherex.caltech.edu/index.html>

The neutral and non-thermal phase of the Universe On the radio side, the leading long-term future facility is the Square Kilometer Array (SKA). Its forecasted Phase 2 improvements in sensitivity below ≤ 200 MHz beyond 2030 will greatly benefit the quest for low surface brightness radio structures in the cosmic web. According to recent numerical simulations, an improvement in sensitivity of a factor ~ 3 should result in a systematic detection of radio emission associated with accretion shocks in the cluster outskirts, as well as in imaging the radio-brightest regions of the larger cosmic web (Vazza et al., 2019). Rare large scale filaments could be detected through the 21cm neutral hydrogen emission line (Horii et al., 2017). The spectroscopic HI galaxy survey is also expected to detect millions of halos, competitive with surveys like Euclid. A reliable catalog of targets expected to be filled with the most rarefied plasmas can be built upon these observations, enabling the physical properties of those plasmas to be revealed at last by further studies, e.g., in X-rays using future missions such as our proposed Cosmic Web Explorer.

5 Executive Summary

We propose a mission concept that provides the necessary combination of X-ray capabilities to answer the most fundamental questions on the distribution, energetic budget and metal enrichment of the hot diffuse matter permeating the Universe’s large-scale structure:

- What are the properties of the soft X-ray emitting halos around L^* galaxies where most of the stars and metals in the Universe were formed? (see Sect. 2.2)
- How does the dynamical assembly of baryons in dark matter halos occur over the entire mass spectrum, from L^* galaxies to galaxy groups to the more massive galaxy clusters? (see Sect. 2.1, 2.2, 2.3)
- What are the complex physical processes affecting both the gas and the stellar components during the accretion of these baryons from the field into virialized structures like galaxies, galaxy groups and clusters? (see Sect. 2.1, 2.2, 2.3)
- What is the role of the poorly understood non-equilibrium physics, which is responsible for the formation and evolution of cosmic structures, in the regions near, and beyond, the virial radii of galaxy groups and clusters? How are they fundamentally different from the physics in the cores of clusters that has been the focus of X-ray cluster science over the past decades? (see Sect. 2.1)
- What are the chemical and thermodynamical properties of the Warm-Hot Intergalactic Medium? How, and where, is it distributed in the local Universe? (see Sect. 2.4)

To reach these goals, starting from the heritage of the ESA L-class mission *Athena*, we need (see Table 1 and Sect. 3):

- a large effective area (~ 10 m² at 1 keV);
- an X-ray Integral Field Unit array with an improved spectral resolution ($E/\Delta E = 2000$) in the soft X-ray band (0.1–3.0 keV);
- high sensitivity (10^{-18} erg cm⁻² s⁻¹ arcmin⁻²), thanks to an unprecedented control on the systematics of the X-ray background that will benefit from a Low-Earth orbit;
- a spatial resolution of 5 arcsec, similar to one achieved by *Athena*, but over a large (~ 1 deg²) FoV.

The combination in a single instrument of all these capabilities will permit a giant leap forward in the complete and exhaustive understanding of the physical processes that shape and define the Cosmic Web, providing the perfect synergetic complement in X-rays to facilities that will be available in other wavebands by 2050, in a joint and harmonious effort to know our Universe in depth.

References

- Abazajian, K., Addison, G., Adshead, P., et al. 2019, arXiv e-prints, arXiv:1907.04473
- Anderson, M. E., Churazov, E., & Bregman, J. N. 2016, MNRAS, 455, 227
- Armillotta, L., Fraternali, F., Werk, J. K., Prochaska, J. X., & Marinacci, F. 2017, MNRAS, 470, 114
- Avestruz, C., Nagai, D., Lau, E. T., & Nelson, K. 2015, ApJ, 808, 176
- Battaglia, N., Bond, J. R., Pfrommer, C., & Sievers, J. L. 2015, ApJ, 806, 43
- Biffi, V., Planelles, S., Borgani, S., et al. 2018, MNRAS, 476, 2689
- Bland-Hawthorn, J., & Gerhard, O. 2016, ARA&A, 54, 529
- Bogdán, Á., Bourdin, H., Forman, W. R., et al. 2017, ApJ, 850, 98
- Borgani, S., Murante, G., Springel, V., et al. 2004, MNRAS, 348, 1078
- Borm, K., Reiprich, T. H., Mohammed, I., & Lovisari, L. 2014, A&A, 567, A65
- Bourne, M. A., & Sijacki, D. 2017, MNRAS, 472, 4707
- Bregman, J. N., Anderson, M. E., Miller, M. J., et al. 2018, ApJ, 862, 3
- Brunetti, G., & Jones, T. W. 2014, International Journal of Modern Physics D, 23, 1430007
- Brunetti, G., & Lazarian, A. 2011, MNRAS, 410, 127
- Bryan, G. L., Norman, M. L., O’Shea, B. W., et al. 2014, ApJS, 211, 19
- Bulbul, E., Gaspari, M., Alvarez, G., et al. 2019, BAAS, 51, 210
- Bykov, A. M., Dolag, K., & Durret, F. 2008, Space Science Reviews, 134, 119
- Bykov, A. M., Vazza, F., Kropotina, J. A., Levenfish, K. P., & Paerels, F. B. S. 2019, Space Science Reviews, 215, 14
- Cen, R., & Chisari, N. E. 2011, ApJ, 731, 11
- Cen, R., & Ostriker, J. P. 2006, ApJ, 650, 560
- Conconi, P., & Campana, S. 2001, A&A, 372, 1088
- Connor, T., Kelson, D. D., Mulchaey, J., et al. 2018, ApJ, 867, 25
- Cotroneo, V., Spiga, D., Barbera, M., et al. 2007, in Proceedings of SPIE, Vol. 6688, Optics for EUV, X-Ray, and Gamma-Ray Astronomy III, 66880U
- Cucchetti, E., Clerc, N., Pointecouteau, E., Peille, P., & Pajot, F. 2019, arXiv e-prints, arXiv:1904.06249
- Eckert, D., Roncarelli, M., Etori, S., et al. 2015a, MNRAS, 447, 2198
- Eckert, D., Vazza, F., Etori, S., et al. 2012, A&A, 541, A57
- Eckert, D., Jauzac, M., Shan, H., et al. 2015b, Nature, 528, 105

- Eckert, D., Gaspari, M., Owers, M. S., et al. 2017, *A&A*, 605, A25
- Eckert, D., Ghirardini, V., Etti, S., et al. 2019, *A&A*, 621, A40
- Eke, V. R., Baugh, C. M., Cole, S., Frenk, C. S., & Navarro, J. F. 2006, *MNRAS*, 370, 1147
- Etti, S., Pratt, G. W., de Plaa, J., et al. 2013, *ArXiv e-prints*, arXiv:1306.2322
- Etti, S., Ghirardini, V., Eckert, D., et al. 2019, *A&A*, 621, A39
- Fraternali, F., & Tomassetti, M. 2012, *MNRAS*, 426, 2166
- Fukugita, M., Hogan, C. J., & Peebles, P. J. E. 1998, *ApJ*, 503, 518
- Fukugita, M., & Peebles, P. J. E. 2006, *ApJ*, 639, 590
- Gaskin, J. A., Allured, R., Bandler, S. R., et al. 2017, in *Society of Photo-Optical Instrumentation Engineers (SPIE) Conference Series*, Vol. 10397, *Society of Photo-Optical Instrumentation Engineers (SPIE) Conference Series*, 103970S
- Gaspari, M., Churazov, E., Nagai, D., Lau, E. T., & Zhuravleva, I. 2014, *A&A*, 569, A67
- Gaspari, M., Ruszkowski, M., & Oh, S. P. 2013, *MNRAS*, 432, 3401
- Ghirardini, V., Eckert, D., Etti, S., et al. 2019, *A&A*, 621, A41
- Govoni, F., Orrù, E., Bonafede, A., et al. 2019, *Science*, 364, 981
- Harrison, F. A., Craig, W. W., Christensen, F. E., et al. 2013, *ApJ*, 770, 103
- Hazumi, M., Ade, P. A. R., Akiba, Y., et al. 2019, *Journal of Low Temperature Physics*, 194, 443
- Hearin, A. P., Zentner, A. R., & Ma, Z. 2012, *JCAP*, 2012, 034
- Hickox, R. C., & Markevitch, M. 2007, *ApJ*, 671, 1523
- Hitomi Collaboration. 2017, *Nature*, 551, 478
- Hitomi Collaboration, Aharonian, F., Akamatsu, H., et al. 2018a, *PASJ*, 70, 11
- . 2018b, *PASJ*, 70, 9
- Hodges-Kluck, E. J., Miller, M. J., & Bregman, J. N. 2016, *ApJ*, 822, 21
- Horii, T., Asaba, S., Hasegawa, K., & Tashiro, H. 2017, *PASJ*, 69, 73
- Irwin, K. D., & Hilton, G. C. 2005, *Transition-Edge Sensors*, ed. C. Enss, Vol. 99 (Springer-Verlag Berlin/Heidelberg), 63
- Irwin, K. D., & Lehnert, K. W. 2004, *Applied Physics Letters*, 85, 2107
- Kaastra, J., Finoguenov, A., Nicastro, F., et al. 2013, *arXiv e-prints*, arXiv:1306.2324
- Kempf, S., Fleischmann, A., Gastaldo, L., & Enss, C. 2018, *Journal of Low Temperature Physics*, 193, 365
- Kereš, D., Katz, N., Weinberg, D. H., & Davé, R. 2005, *MNRAS*, 363, 2
- Khatri, R., & Gaspari, M. 2016, *MNRAS*, 463, 655

- Klaassen, P., Mroczkowski, T., Bryan, S., et al. 2019, arXiv e-prints, arXiv:1907.04756
- Lau, E. T., Gaspari, M., Nagai, D., & Coppi, P. 2017, ApJ, 849, 54
- Lau, E. T., Kravtsov, A. V., & Nagai, D. 2009, ApJ, 705, 1129
- Le Brun, A. M. C., McCarthy, I. G., Schaye, J., & Ponman, T. J. 2014, MNRAS, 441, 1270
- Lee, S. J., Adams, J. S., Bandler, S. R., et al. 2015, Applied Physics Letters, 107, 223503
- Li, J.-T., Bregman, J. N., Wang, Q. D., Crain, R. A., & Anderson, M. E. 2018, ApJ, 855, L24
- Mates, J. A. B., Hilton, G. C., Irwin, K. D., Vale, L. R., & Lehnert, K. W. 2008, Applied Physics Letters, 92, 023514
- Maughan, B. J., Giles, P. A., Randall, S. W., Jones, C., & Forman, W. R. 2012, MNRAS, 421, 1583
- McNamara, B. R., Russell, H. R., Nulsen, P. E. J., et al. 2016, ApJ, 830, 79
- McQuinn, M., & Werk, J. K. 2018, ApJ, 852, 16
- Merloni, A., Predehl, P., Becker, W., et al. 2012, arXiv e-prints, arXiv:1209.3114
- Mernier, F., Biffi, V., Yamaguchi, H., et al. 2018a, Space Science Reviews, 214, 129
- Mernier, F., de Plaa, J., Werner, N., et al. 2018b, ArXiv e-prints, arXiv:1803.06296
- Molnar, S. M., Hearn, N., Haiman, Z., et al. 2009, ApJ, 696, 1640
- Morandi, A., & Cui, W. 2014, MNRAS, 437, 1909
- Moseley, S. H., Mather, J. C., & McCammon, D. 1984, Journal of Applied Physics, 56, 1257
- Mroczkowski, T., Nagai, D., Basu, K., et al. 2019, Space Science Reviews, 215, 17
- Mushotzky, R. 2018, in Society of Photo-Optical Instrumentation Engineers (SPIE) Conference Series, Vol. 10699, Society of Photo-Optical Instrumentation Engineers (SPIE) Conference Series, 1069929
- Nagai, D., & Lau, E. T. 2011, ApJ, 731, L10
- Naidoo, K., Whiteway, L., Massara, E., et al. 2019, arXiv e-prints, arXiv:1907.00989
- Nandra, K., Barret, D., Barcons, X., et al. 2013, arXiv e-prints, arXiv:1306.2307
- Nelson, D., Kauffmann, G., Pillepich, A., et al. 2018, MNRAS, 477, 450
- Nelson, K., Lau, E. T., Nagai, D., Rudd, D. H., & Yu, L. 2014, ApJ, 782, 107
- Nevalainen, J., Tempel, E., Liivamägi, L. J., et al. 2015, A&A, 583, A142
- Nicastro, F., Kaastra, J., Krongold, Y., et al. 2018, Nature, 558, 406
- Oppenheimer, B. D. 2018, MNRAS, 480, 2963
- Oppenheimer, B. D., Segers, M., Schaye, J., Richings, A. J., & Crain, R. A. 2018, MNRAS, 474, 4740
- Oppenheimer, B. D., Crain, R. A., Schaye, J., et al. 2016, MNRAS, 460, 2157

- Osmond, J. P. F., & Ponman, T. J. 2004, *MNRAS*, 350, 1511
- Ota, N., Nagai, D., & Lau, E. T. 2018, *PASJ*, 70, 51
- Pareschi, G., Cotroneo, V., Spiga, D., et al. 2004, in *Society of Photo-Optical Instrumentation Engineers (SPIE) Conference Series*, Vol. 5488, *Proceedings of SPIE*, 481–491
- Pellegrini, S., Ciotti, L., Negri, A., & Ostriker, J. P. 2018, *ApJ*, 856, 115
- Pezzulli, G., Fraternali, F., & Binney, J. 2017, *MNRAS*, 467, 311
- Pillepich, A., Reiprich, T. H., Porciani, C., Borm, K., & Merloni, A. 2018a, *MNRAS*, 481, 613
- Pillepich, A., Springel, V., Nelson, D., et al. 2018b, *MNRAS*, 473, 4077
- Pisani, A., Massara, E., Spergel, D. N., et al. 2019, in *BAAS*, Vol. 51, 40
- Planelles, S., Borgani, S., Fabjan, D., et al. 2014, *MNRAS*, 438, 195
- Pointecouteau, E., Reiprich, T. H., Adami, C., et al. 2013, *arXiv e-prints*, arXiv:1306.2319
- Ponti, G., Hofmann, F., Churazov, E., et al. 2019, *Nature*, 567, 347
- Pratt, G. W., Croston, J. H., Arnaud, M., & Böhringer, H. 2009, *A&A*, 498, 361
- Roncarelli, M., Cappelluti, N., Borgani, S., Branchini, E., & Moscardini, L. 2012, *MNRAS*, 424, 1012
- Roncarelli, M., Ettori, S., Borgani, S., et al. 2013, *MNRAS*, 432, 3030
- Roncarelli, M., Moscardini, L., Tozzi, P., et al. 2006, *MNRAS*, 368, 74
- Roncarelli, M., Gaspari, M., Ettori, S., et al. 2018, *A&A*, 618, A39
- Rudd, D. H., & Nagai, D. 2009, accepted to the *ApJL*, arXiv:0907.1287
- Ryu, D., Kang, H., Hallman, E., & Jones, T. W. 2003, *ApJ*, 593, 599
- Sauvageot, J. L., de la Broïse, X., Charvolin, T., et al. 2018, in *Society of Photo-Optical Instrumentation Engineers (SPIE) Conference Series*, Vol. 10699, *Proceedings of SPIE*, 106992I
- Sauvageot, J. L., Pigot, C., de la Broïse, X., et al. 2016, in *Society of Photo-Optical Instrumentation Engineers (SPIE) Conference Series*, Vol. 9905, *Proceedings of SPIE*, 99050S
- Schaye, J., Crain, R. A., Bower, R. G., et al. 2015, *MNRAS*, 446, 521
- Sehgal, N., Aiola, S., Akrami, Y., et al. 2019, *arXiv e-prints*, arXiv:1906.10134
- Shi, X., Komatsu, E., Nelson, K., & Nagai, D. 2015, *MNRAS*, 448, 1020
- Shi, X., Nagai, D., & Lau, E. T. 2018, *MNRAS*, 481, 1075
- Shull, J. M., Danforth, C. W., & Tilton, E. M. 2014, *ApJ*, 796, 49
- Siegel, S. R., Sayers, J., Mahdavi, A., et al. 2018, *ApJ*, 861, 71
- Simionescu, A., Werner, N., Mantz, A., Allen, S. W., & Urban, O. 2017, *MNRAS*, 469, 1476
- Simionescu, A., Werner, N., Urban, O., et al. 2015, *ApJ*, 811, L25

Simionescu, A., Allen, S. W., Mantz, A., et al. 2011, *Science*, 331, 1576

Simionescu, A., Werner, N., Urban, O., et al. 2013, *ApJ*, 775, 4

Smith, S. J., Adams, J. S., Bandler, S. R., et al. 2019, *Journal of Astronomical Telescopes, Instruments, and Systems*, 5, 021008

Spiga, D. 2011, *A&A*, 529, A18

Stern, J., Hennawi, J. F., Prochaska, J. X., & Werk, J. K. 2016, *ApJ*, 830, 87

Sun, M. 2012, *New Journal of Physics*, 14, 045004

Sunyaev, R. A., & Zeldovich, Y. B. 1972, *A&A*, 20, 189

Tanimura, H., Aghanim, N., Douspis, M., Beelen, A., & Bonjean, V. 2019, *A&A*, 625, A67

Tchernin, C., Eckert, D., Ettore, S., et al. 2016, *A&A*, 595, A42

Tempel, E., Kipper, R., Saar, E., et al. 2014, *A&A*, 572, A8

The LUVOIR Team. 2018, arXiv e-prints, arXiv:1809.09668

The Simons Observatory Collaboration, Abitbol, M. H., Adachi, S., et al. 2019, arXiv e-prints, arXiv:1907.08284

Truong, N., Rasia, E., Mazzotta, P., et al. 2018, *MNRAS*, 474, 4089

Tumlinson, J., Thom, C., Werk, J. K., et al. 2011, *Science*, 334, 948

Ullom, J. N., & Bennett, D. A. 2015, *Superconductor Science Technology*, 28, 084003

Urban, O., Werner, N., Allen, S. W., Simionescu, A., & Mantz, A. 2017, *MNRAS*, 470, 4583

Urban, O., Simionescu, A., Werner, N., et al. 2014, *MNRAS*, 437, 3939

Ursino, E., Galeazzi, M., & Huffenberger, K. 2014, *ApJ*, 789, 55

Ursino, E., Galeazzi, M., & Roncarelli, M. 2010, *ApJ*, 721, 46

van Daalen, M. P., McCarthy, I. G., & Schaye, J. 2019, arXiv e-prints, arXiv:1906.00968

van Daalen, M. P., & Schaye, J. 2015, *MNRAS*, 452, 2247

van der Wel, A., Franx, M., van Dokkum, P. G., et al. 2014, *ApJ*, 788, 28

Vazza, F., Angelinelli, M., Jones, T. W., et al. 2018, *MNRAS*, 481, L120

Vazza, F., Brüggén, M., Gheller, C., et al. 2017, *Classical and Quantum Gravity*, 34, 234001

Vazza, F., Eckert, D., Simionescu, A., Brüggén, M., & Ettore, S. 2013, *MNRAS*, 429, 799

Vazza, F., Ettore, S., Roncarelli, M., et al. 2019, arXiv e-prints, arXiv:1903.04166

Vogelsberger, M., Genel, S., Springel, V., et al. 2014, *MNRAS*, 444, 1518

Voit, G. M., Donahue, M., O’Shea, B. W., et al. 2015, *ApJ*, 803, L21

Walker, S., Simionescu, A., Nagai, D., et al. 2019, *Space Science Reviews*, 215, 7

- Werk, J. K., Prochaska, J. X., Cantalupo, S., et al. 2016, *ApJ*, 833, 54
- Werner, N., Finoguenov, A., Kaastra, J. S., et al. 2008, *A&A*, 482, L29
- Werner, N., Urban, O., Simionescu, A., & Allen, S. W. 2013, *Nature*, 502, 656
- Yamada, S., Ohashi, T., Ishisaki, Y., et al. 2018, *Journal of Low Temperature Physics*,
doi:10.1007/s10909-018-1918-z
- Zhuravleva, I., Churazov, E., Kravtsov, A., et al. 2013, *MNRAS*, 428, 3274
- Zhuravleva, I., Churazov, E., Schekochihin, A. A., et al. 2014, *Nature*, 515, 85
- Zinger, E., Dekel, A., Birnboim, Y., Kravtsov, A., & Nagai, D. 2016, *MNRAS*, 461, 412
- Zinger, E., Dekel, A., Birnboim, Y., et al. 2018, *MNRAS*, 476, 56
- ZuHone, J. A., Markevitch, M., & Zhuravleva, I. 2016, *ApJ*, 817, 110